Tetrameric UvrD helicase is located at the *E. coli* replisome due to frequent replication blocks

Adam J. M Wollman[1,2,3,], Aisha H. Syeda[1,2], Jamieson A. L. Howard[1,2], Alex Payne-Dwyer[1,2], Andrew Leech[4] , Colin Guy[5, 6], Peter McGlynn[2,6], Michelle Hawkins[2] and Mark C. Leake[1,2]

The authors wish it to be known that, in their opinion, the first two authors should be regarded as joint First Authors

[1] School of Physics, Engineering and Technology, University of York, York YO10 5DD, United Kingdom.

[2] Department of Biology, University of York, York YO10 5DD, United Kingdom.

[3] Current address: Biosciences Institute, Newcastle University, NE1 7RU, United Kingdom.

[4] Bioscience Technology Facility, Department of Biology, University of York, York YO10 5DD, United Kingdom

[5] Current address: Covance Laboratories Ltd., Otley Road, Harrogate, HG3 1PY, United Kingdom

[6] Previous address: School of Medical Sciences, Institute of Medical Sciences, University of Aberdeen, Foresterhill, Aberdeen AB25 2ZD, United Kingdom

* To whom correspondence should be addressed. To whom correspondence should be addressed. Tel: +44 (0)1904322697. Email: mark.leake@york.ac.uk

Present Address: School of Physics, Engineering and Technology, and Department of Biology, University of York, York YO10 5DD, United Kingdom

SUMMARY

DNA replication in all organisms must overcome nucleoprotein blocks to complete genome duplication. Accessory replicative helicases in *Escherichia coli*, Rep and UvrD, help replication machinery overcome blocks by removing incoming nucleoprotein complexes or aiding the re-initiation of replication. Mechanistic details of Rep function have emerged from recent live cell studies; however, the division of UvrD between its multiple activities in DNA repair and its role as an accessory helicase remains unclear in live cells. Here, by integrating super-resolved single-molecule fluorescence microscopy with biochemical analysis, we find that UvrD self-associates into a tetramer and, unlike Rep, is not recruited to a specific replisome protein despite being found at approximately 80% of replication forks. Instead, its recruitment to forks is likely mediated by the very high frequency of replication blocks due to DNA bound proteins, including RNA polymerase and DNA damage. Deleting *rep* and DNA repair factor genes *mutS* and *uvrA*, and inhibiting transcription through RNA polymerase

mutation and antibiotic inhibition, indicates that the level of UvrD at the fork is dependent on its function. Our findings show that UvrD is recruited to sites of nucleoprotein blocks via distinctly different mechanisms to Rep and plays a multi-faceted role in ensuring successful DNA replication.

INTRODUCTION

Replication and transcription of DNA occur simultaneously in *Escherichia coli,* making conflicts between the bacterial replisome, the molecular replication machine comprising in excess of 10 different proteins, and RNA polymerase (RNAP) inevitable (1–4). Collisions between the replication and transcription machineries hinder replication fork progression and cause genome instability (5–14). RNAP can pause, stall and backtrack while actively transcribing, and any immobile RNAP molecules present long-lived barriers to replisomes (15, 16). These factors make RNAP the most common nucleoprotein obstacle for translocating replisomes. DNA is also frequently damaged in normal growth conditions due to exposure to endogenous and exogenous DNA damaging agents. The resulting DNA damage also presents significant obstacles for normal replication (17–19).

Several mechanisms exist to reduce conflict between the replisome and obstacles such as transcribing RNAPs. For example, transcription elongation and termination factors reduce the number of immobile RNA polymerases on DNA (1, 18, 20–24). Head-on collisions were originally thought to be more harmful (25–27) and therefore more important to resolve; a view supported by the occurrence of highly transcribed genes encoded on the leading strand, presumably to ensure co-directional transcription and replication (26, 28, 29). However, co-directional collisions of the replisome and transcription machinery also impact replication fork progression (3, 18, 30).

Accessory replicative helicases promote fork movement through nucleoprotein barriers and have been identified in prokaryotes and eukaryotes (1, 12, 13, 31, 32). The Rep and UvrD accessory helicases in *E. coli*, as well as the Pif1 helicase in *Saccharomyces cerevisiae*, perform important roles in helping to clear nucleoprotein complexes (33). More recently, Pif1 has been proposed to be a general displacement helicase for replication bypass of protein blocks, a function similar to the Rep and UvrD helicases (34). These helicases can reduce replisome pausing at several types of

70 native transcription complexes observed in living cells (13, 22, 35), and several types
71 of engineered nucleoprotein blocks in biochemical experiments *in vitro* (1, 31).
72 Rep is the primary accessory helicase in *E. coli*, however, UvrD can partially
73 compensate for the absence of Rep *in vivo* and has been shown to promote replication
74 through stalled transcription elongation complexes (1, 12, 13, 36, 37). UvrD is a
75 superfamily 1 helicase that translocates 3'-5' along ssDNA. The ability of UvrD to
76 compensate partially for the absence of Rep has been attributed to the high degree of
77 homology between these two helicases and the abundance of UvrD inside cells (12,
78 21, 38–40). The role of UvrD in nucleotide excision repair along with UvrABC proteins
79 as well as in methyl-directed mismatch repair along with the MutHLS proteins is well
80 characterised (41–46). UvrD interacts directly with RNAP but the functional
81 importance of this interaction has been unclear until recently (47–50). UvrD has been
82 suggested to promote backtracking of stalled RNAP as a first step in transcription-
83 coupled repair (50, 51); however, other studies argue against UvrD playing any role in
84 coupling nucleotide excision repair to stalled transcription complexes (48, 49, 52–56).
85 Here, we combined state-of-the-art live cell imaging using single-molecule
86 microscopy with advanced biochemical activity experiments *in vitro* to elucidate how
87 UvrD resolves replicative blocks. We used super-resolved high-speed single-molecule
88 fluorescence microscopy of mGFP-UvrD in live cells co-expressing a fork marker,
89 DnaQ-mCherry, to reveal that 80% of DnaQ foci colocalise with UvrD. Stepwise
90 photobleaching intensity analysis showed that UvrD is a tetramer *in vivo*, to be
91 compared with earlier observations performed *in vitro* using analytical
92 ultracentrifugation that found a mixture of UvrD dimers and tetramers (57). Surface
93 plasmon resonance (SPR) measurements of UvrD in combination with each replisome
94 component identified no specific replisome protein interaction partner that would
95 explain replisome-UvrD colocalisation. Deletion of Rep, mismatch repair protein MutS
96 and nucleotide excision repair protein UvrA, and disruption of transcription using either
97 mutation of RNAP or antibiotic inhibition, significantly reduces the number of UvrD or
98 level of observed colocalisation of UvrD with the fork. Coupled with *in vitro* block-
99 dependent differences in UvrD replication promotion efficiency, we conclude that UvrD
100 is located at the *E. coli* replisome due to its role in resolving frequent blocks to
101 replication.
102
103

RESULTS

UvrD is present at the majority of replication forks

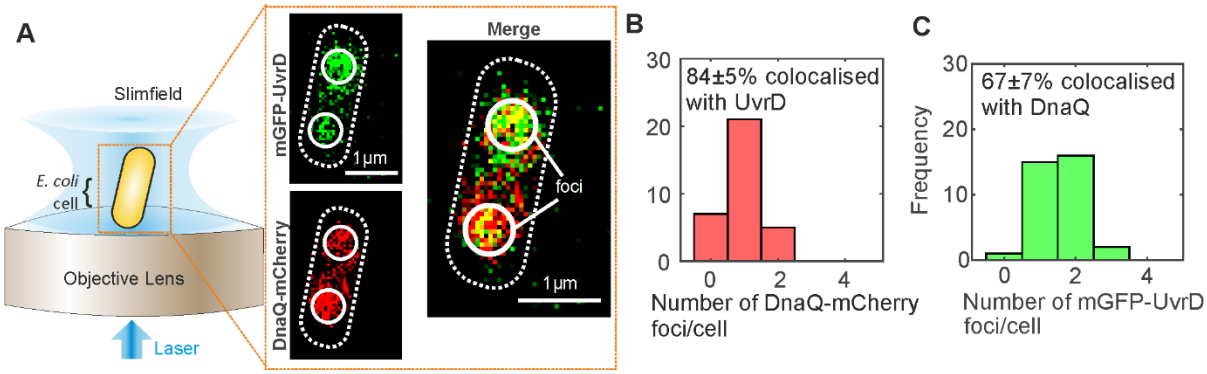

Figure 1: Super-resolved single-molecule light microscopy. (A). Slimfield microscope schematic and Slimfield micrographs of mGFP-UvrD, DnaQ-mCherry. Cell membrane and DnaQ/UvrD foci indicated as white dashed and non-dashed lines respectively. (B) and (C) Histogram showing the number of DnaQ and UvrD foci detected per cell respectively, SD errors.

We investigated the role of UvrD in DNA replication using super-resolved single-molecule fluorescence microscopy to track dynamic patterns of fluorescently labelled UvrD localization relative to the replication fork in live cells (Figure 1A). We performed dual-colour Slimfield (63, 78) to assess the degree of colocalisation between UvrD and the replisome, using a similar imaging protocol as previously for Rep (13). We employed DnaQ-mCherry as a fork marker (13) along with a genomically integrated mGFP-UvrD fluorescent protein fusion construct to report on the localization of UvrD. DnaQ encodes the epsilon subunit, a core component of the DNA polymerase and is well established as a marker for the replication fork (13, 69, 79–81). These strains phenocopied the wild type strain for growth and in plasmid loss assays testing for mGFP-UvrD function retention (Supplementary Figures S1, S2, Tables S1-4). The helicase activity of mGFP-UvrD was comparable to the wild type enzyme in an *in vitro* unwinding assay (Supplementary Figure S3). Under Slimfield, we observed 1-2 DnaQ foci as in the previous study for Rep, corresponding to the two moving replication forks which appear as single foci near the start of replication when they are separated by less than the 200-300 nm diffraction limit of our microscope (Figure 1A,B Supplementary Figure S4). We also observed 1-2 UvrD foci per cell, of which 67 ± 7% (±SEM) were colocalised with DnaQ foci and 84 ± 5% of DnaQ foci were colocalised with UvrD (Figure 1B and C). We calculated the probability of random overlap between these foci, by modelling the nearest-neighbour foci separation as a Poisson

133 distribution (70), to be 20%. To confirm that colocalisation between DnaQ and UvrD
134 was not just a function of the nucleoid association of UvrD, we performed Slimfield
135 imaging of Heat-stable nucleoid-structuring protein (H-NS) tagged with GFP dual
136 labelled with DnaQ-mCherry. H-NS associates with the nucleoid but not specifically
137 with the fork. We found similar numbers of H-NS foci (Supplementary Figure S5) but
138 only 38±4% DnaQ foci were colocalised with H-NS implying that, similarly to the Rep
139 helicase (13), UvrD is present at the majority of replication forks.
140
141 **UvrD is a tetramer in live bacterial cells**
142

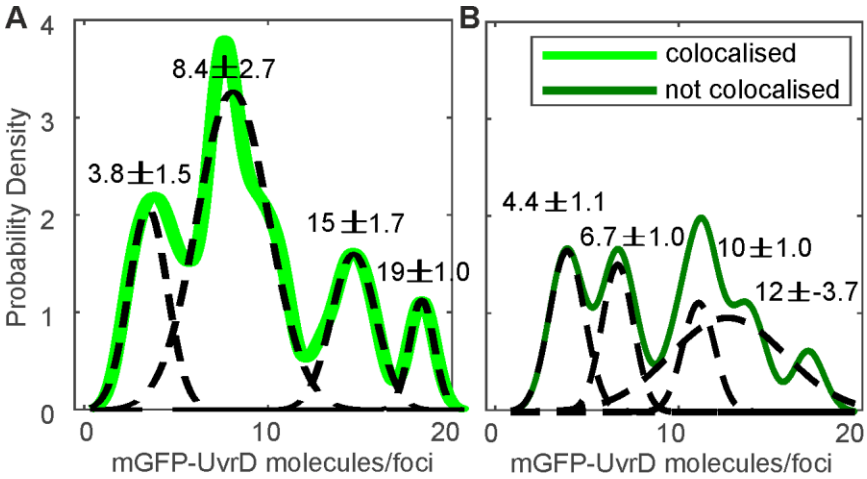

143
144 **Figure 2 UvrD stoichiometry.** The distribution of UvrD foci stoichiometry rendered as a
145 kernel density estimate for foci colocalised (A) and not colocalised (B) with DnaQ foci.
146 Distributions were fitted with multiple Gaussian peaks (black dotted lines) with the peak value
147 ± error determined by the half width at half maximum indicated above each peak
148
149 Slimfield also enabled the stoichiometry of these foci to be determined by utilizing a
150 method involving step-wise photobleaching analysis (69). Here, we determined the
151 brightness of a single-molecule of mGFP or mCherry fluorescent protein under our
152 Slimfield imaging conditions (Supplementary Figure S7), and used these values to
153 normalize the initial brightness of all tracked foci as an estimate for the apparent
154 stoichiometry in terms of number of fluorescently labelled molecules present. We
155 found that DnaQ had the same range of 2-6 molecules per focus (Supplementary
156 Figure S8) as we have found previously, corresponding to 2-3 polymerases per fork
157 (13, 69). The distribution of the apparent stoichiometry of UvrD foci which are
158 colocalised with DnaQ had a distinct lowest-order peak corresponding to
159 approximately four molecules, with subsequent peaks at clear multiples of four (Figure

160 2A). UvrD foci that are not colocalised with DnaQ also contained a distinct lowest-
161 order peak at four, but subsequent peaks were less clearly tetrameric. We performed
162 Size Exclusion Chromatography - Multi-Angle Laser Light Scattering (SEC-MALLS) to
163 test whether the fluorescent protein labelling UvrD might be inducing multimers but
164 found limited effects on UvrD assembly state, as expected from the K_D dissociation
165 constant of fluorescent proteins containing the A206K mutation (82) (Supplementary
166 Figure S9). UvrD has been shown to exist in a monomer-dimer-tetramer equilibrium
167 *in vitro* (57). DNA unwinding experiments *in vitro* suggest UvrD must function as at
168 least a dimer (83) or a trimer (84), however the oligomeric state of functional UvrD is
169 disputed (reviewed in (85)). To our knowledge, these are the first UvrD stoichiometry
170 measurements *in vivo* so we propose that UvrD forms a tetramer *in vivo* with multiple
171 tetramers often at the replication fork. It should be noted that we often observe only a
172 single DnaQ focus corresponding to two replication forks which are separated by less
173 than the diffraction limit of our microscope (Supplementary Figure S8) such that some
174 multiple tetramer UvrD foci correspond to two replication forks. The less distinct peaks
175 in the UvrD foci that are not colocalised with DnaQ may indicate that other UvrD
176 species (monomers, dimers or trimers) are also present.
177 We were also able to determine the total cell copy number of UvrD using a
178 method which determined the total contribution of mGFP-UvrD fluorescence to the
179 observed intensity in whole cells (72). We found approximately 800 molecules of UvrD
180 per cell (Supplementary Figure S10), similar to that which we reported previously for
181 Rep (13). This is a much lower level of UvrD than was reported using transcription rate
182 measurements (86) or high-throughput proteomics (87) but is comparable to recent
183 estimates using ribosome profiling (88).
184
185 **No interaction partner was found for UvrD at the fork with SPR**
186 Our earlier findings concerning the accessory helicase Rep indicated that
187 colocalisation with the fork and recruitment to the replisome were mediated by specific
188 interaction with the replicative helicase DnaB (89), with Rep and DnaB both exhibiting
189 hexameric stoichiometry (13, 69). We sought to determine whether UvrD is also
190 recruited by interacting with a specific replisome component using SPR on purified
191 UvrD and each replisome component (Supplementary Figure 11). UvrD exhibited no
192 direct interaction with primase, SSB, β sliding clamp, the DNA polymerase III αε, χψ
193 or γ complexes; or θ, δ, δ′, χ, and γ subunits (12). We did initially identify a putative

weak UvrD-Tau interaction. However, as a control we also tested Rep, and found this also interacted with Tau to a similar extent, and with ~100x lower affinity than UvrD with known interaction partner UvrB (Supplementary Figure 8). We therefore conclude that the Tau interaction with UvrD is non-specific and that, unlike Rep, UvrD likely does not have a direct interaction partner at the replisome from the suite of replisome proteins tested. As UvrD is a tetramer at the replisome, it is also unlikely to be recruited by Rep, which has shown putative interaction (90).

UvrD presence at the replication fork is mediated by specific blocks to replication

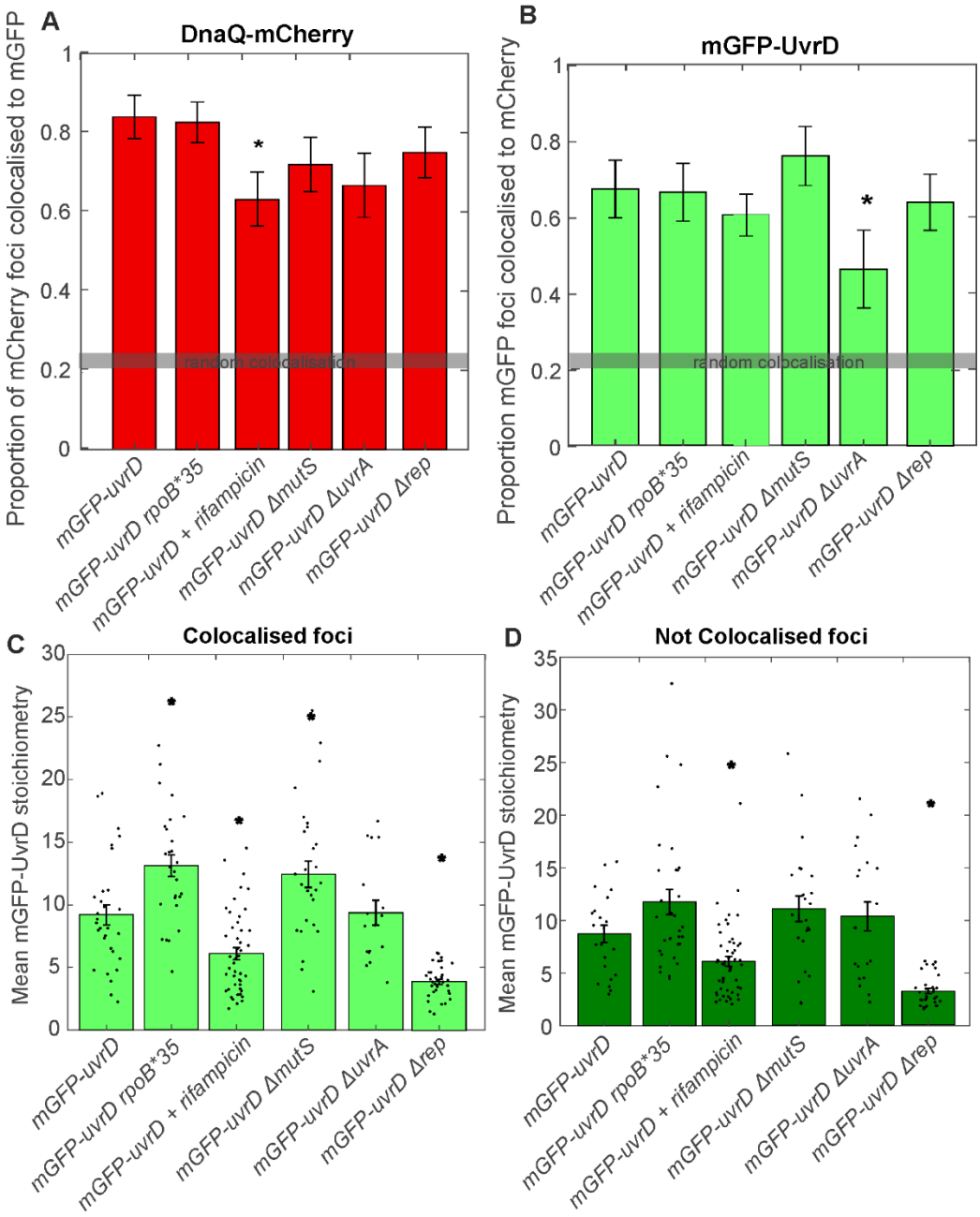

205 **Figure 3: UvrD perturbations.** A. and B. The mean proportion of colocalised DnaQ and UvrD
206 foci per cell respectively. Error bars represent standard error in the mean and statistical
207 significance by Student's t-test $p<0.05$ indicated by *. C. and D. Jitter plots of colocalised and
208 not colocalised UvrD stoichiometry respectively. Bars show mean UvrD stoichiometry with
209 error bars showing the standard error in the mean and statistical significance by Student's t-
210 tests $p<0.05$ indicated by *.
211
212 Since our SPR observations indicated that UvrD does not interact directly and
213 specifically with any core replisome protein, we hypothesized that the association of
214 UvrD with the replication fork might be dependent on its activity in resolving
215 nucleoprotein blocks. To test this, we systematically impaired key DNA replication
216 repair processes in which UvrD is implicated, as well as perturbing RNAP replicative
217 blocks by disruption of transcription through both genetic mutation and antibiotic
218 inhibition (Figure 3). We perturbed UvrD's activity in resolving DNA damage at
219 replication blocks by deleting *mutS* or *uvrA*, rendering the strains defective in UvrD-
220 associated mismatch repair or nucleotide excision repair respectively (43, 91). We
221 reduced the need for UvrD to remove transcriptional blocks to replication (49) by
222 introducing the *rpoB*35* mutation, which destabilizes open complexes formed during
223 initiation of transcription (92, 93); and by using the antibiotic rifampicin, which blocks
224 elongation of RNA transcripts (94). All of these strains were healthy under normal
225 growth conditions (Supplementary Figure S1, Table S4) and displayed the same
226 phenotype for DnaQ foci number and stoichiometry within measurement error
227 (Supplementary Figure S8).
228 For the transcriptional block perturbations, the *rpoB*35* mutant dual labelled
229 strain exhibited no difference in the proportion of colocalised DnaQ or UvrD foci
230 (Figure 3A and B). This mutant and all others tested exhibited the same predominant
231 tetrameric stoichiometry trends as wild type (Supplementary Figure S12), with clear
232 peaks at tetramer intervals in the colocalised stoichiometry distribution and less clear
233 but still largely tetrameric intervals in the stoichiometry distribution for UvrD foci that
234 are not colocalised with DnaQ. This provides further evidence that UvrD operates
235 predominantly as a tetramer *in vivo*. We compared the mean stoichiometry for each
236 mutant to that of wild type (Figure 3C and D). Unexpectedly, the *rpoB*35* mutant
237 produced a slight but statistically significant increase in mean colocalised
238 stoichiometry, corresponding to approximately one extra UvrD tetramer at the
239 replication fork (Figure 3C). This finding may indicate the level of instability conferred
240 by this mutation has multiple downstream effects that alter UvrD localisation

241 significantly at the fork. Alternatively, it could mean that *rpoB*35* does not affect the
242 formation of the types of transcriptional block that are acted upon by UvrD. Rifampicin
243 treatment produced a clearer response, reducing the number of DnaQ foci colocalised
244 with UvrD by ~20% (Figure 3A) and the mean stoichiometry of colocalised and not
245 colocalised UvrD foci by around one UvrD tetramer (Figure 3C and D). Single-
246 molecule observations of RNAP have shown it to be significantly more mobile under
247 rifampicin treatment (95), implying fewer RNAPs bound to DNA and fewer blocks to
248 replication. Our rifampicin treatment results are consistent with fewer transcriptional
249 blocks to replication reducing the amount of UvrD recruited to the replisome and
250 support the hypothesis that UvrD is recruited by these replicative blocks.
251 By deleting *mutS* or *uvrA* we removed UvrD's role in mismatch repair and
252 nucleotide excision repair respectively. Deleting *mutS* surprisingly resulted in no
253 change in UvrD colocalisation with DnaQ but did increase the mean UvrD
254 stoichiometry colocalised with DnaQ by around one tetramer (Figure 3A). In the Δ*uvrA*
255 mutant this resulted in a clear drop of ~25% in UvrD colocalisation with DnaQ (Figure
256 3B) with no change in the number of UvrD foci (Supplementary Figure S8), consistent
257 with the hypothesis that UvrD association with the fork is dependent on actively
258 resolving DNA damage induced blocks to replication. The minimal response in the
259 Δ*mutS* strain may also suggest that UvrD at the fork is more involved in nucleotide
260 excision repair than mismatch repair.
261 UvrD has been shown to compensate for Rep in *rep* null mutants (12). We also
262 tested what effect this mutation would have in our single-molecule assay. Surprisingly,
263 *rep* deletion resulted in a steep drop in UvrD copy number (Supplementary Figure
264 S10). The degree of colocalisation between UvrD and DnaQ remained unchanged
265 compared to wild type (Figure 3A and B) but the stoichiometry of foci was reduced to
266 a single UvrD tetramer (Figure 3C and D and Supplementary Figure 11), presumably
267 due to the lower copy number and availability of UvrD. The drop in UvrD copy number
268 may reflect complex regulatory shifts in response to losing such a key protein in Rep,
269 although it is interesting that even at low copy numbers, a UvrD tetramer remains
270 recruited to the fork. Double knockouts, deficient in both Rep and UvrD, are lethal (12)
271 so this minimal helicase presence must be the limit required for survival.
272

The dynamic association of UvrD with the replication fork is dependent on repair processing

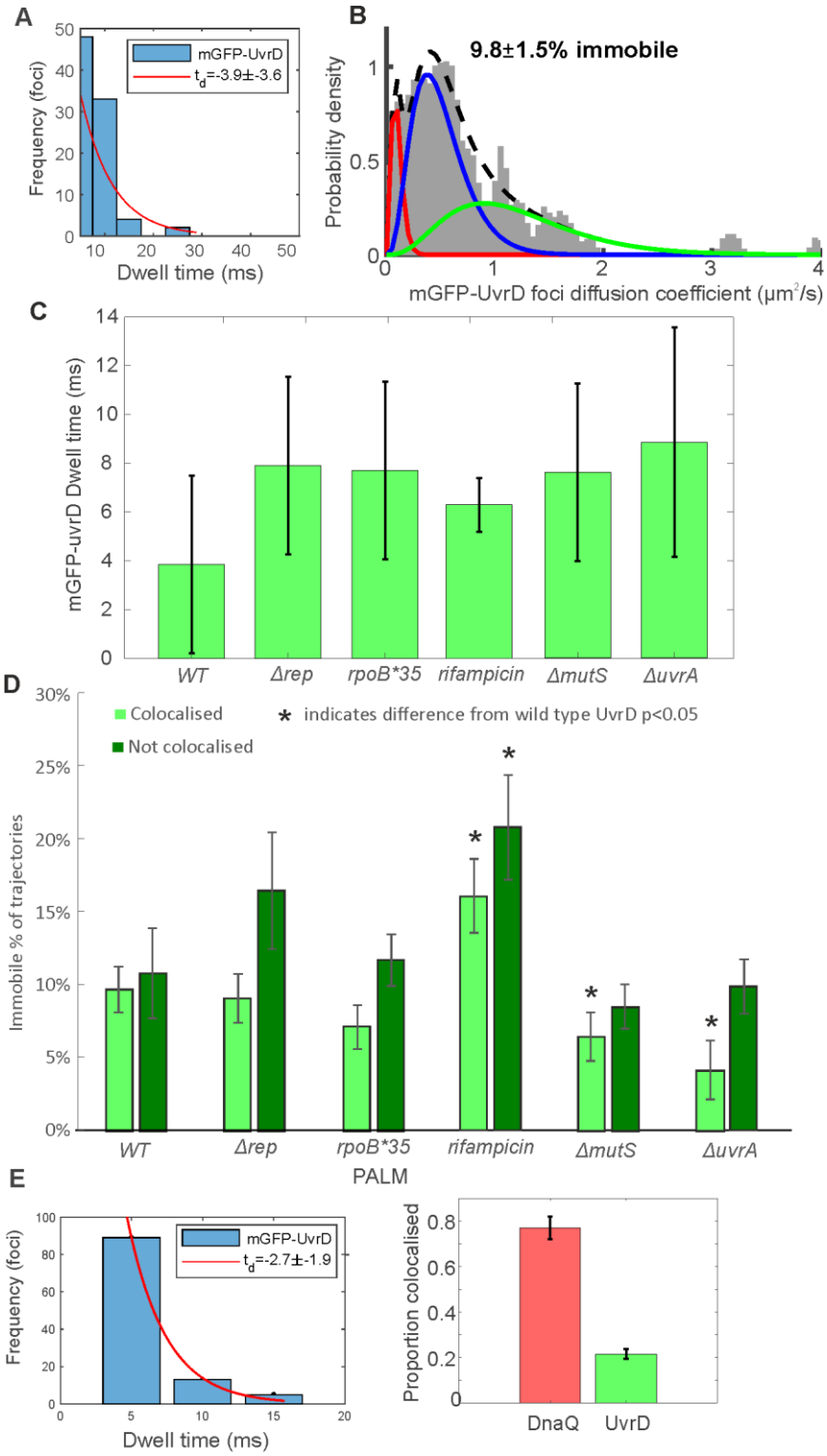

Figure 4: UvrD dynamics. A. Distribution of time over which UvrD and DnaQ foci were colocalised (blue) fitted with an exponential (red) to yield a characteristic dwell time. B. Distribution of microscopic diffusion coefficients of wild type UvrD foci (grey) fitted with a three state gamma distribution model containing a relatively immobile population with $D = 0.1$ μm²/s (red), a transiently immobile population, $D = 0.5$ μm²/s (blue) and a mobile population,

281 D=1.2 μm^2/s (green). C. The dwell times for each UvrD strain. Error bars represent the 95%
282 confidence intervals on the fit. D. The proportion of UvrD foci in the immobile population for
283 each UvrD strain colocalised or not colocalised with DnaQ foci location. Statistically
284 significant differences $p<0.05$ from wild type indicated by *. E. PALM dwell time and
285 colocalisation proportion of detected tracks.
286

287 By tracking UvrD foci as a function of time using rapid millisecond timescale sampling
288 in Slimfield imaging, we were also able to characterize its dynamics in wild type and
289 repair impaired cells. We measured the number of frames UvrD foci were colocalised
290 with DnaQ foci positions, the dwell time, and calculated the apparent microscopic
291 diffusion coefficient of individual foci (Figure 4 and Supplementary Figure S13). The
292 UvrD dwell time at the fork for the wild type strain was measured to be approximately
293 4 ms, indicating a relatively dynamic association of UvrD at the replication fork. The
294 apparent microscopic diffusion coefficients (*D*) were best fit with a three parameter
295 Gamma model, containing a relatively immobile population with $D = 0.1$ μm^2/s, a
296 transiently immobile population, $D = 0.5$ μm^2/s and a mobile population, D=1.2 μm^2/s,
297 similar to Rep (13). In wild type, we found approximately 10% of UvrD foci were
298 immobile, whether colocalised with the DnaQ fork location or not, with the rest of the
299 foci split between the other two populations.
300 We sought to use these molecular measurements to determine the effect of
301 perturbing UvrD-mediated DNA replication repair and block resolution on UvrD
302 dynamics. All deletions resulted in a marginal though statistically negligible increase
303 in dwell time to between 6-9 ms. The Δ*rep* and *rpoB*35* mutations resulted in no
304 change in mobility from wild type. Rifampicin treatment however, resulted in an
305 increase in the proportion of immobile foci both at and away from the fork. This finding
306 appears counterintuitive as rifampicin treatment results in more mobile RNAP (95),
307 however it is unclear what effect rifampicin has on the population of RNAP molecules
308 that remain bound to DNA. These results may suggest that such blocks provide an
309 increased barrier to replication, decreasing mobility of UvrD as it attempts to deal with
310 these blocks. In the Δ*mutS* and Δ*uvrA* strains, the proportion of immobile foci
311 decreased at the fork, again consistent with the hypothesis that UvrD association with
312 the fork is dependent on DNA damage resolution activity. An alternative explanation
313 for these results is that UvrD is less mobile when resolving DNA damage blocks to
314 replication and more mobile when resolving transcriptional blocks, as reducing or

315 eliminating UvrD's role in these processes decreased or increased the immobile
316 fraction in DNA repair and transcription impaired cells respectively (Figure 4).
317
318 ***In vitro* experiments confirm block-dependent UvrD function**
319 To further investigate the role of blocks in UvrD recruitment to the replisome, we
320 performed a stalled replication assay *in vitro,* which allowed us to specifically vary the
321 nucleoprotein block and the timing of UvrD recruitment i.e. before or after the
322 replisome had encountered the block. *E. coli* replisomes can be reconstituted on
323 plasmid DNA templates containing *oriC* and engineered stall sites. UvrD can be
324 included from the start of replication or added after the replisome has encountered the
325 nucleoprotein block. Blocked fork resolution was then probed by examining replication
326 products by denaturing gel electrophoresis.
327 We first used an *oriC*-containing plasmid which contained a specific RNAP stall
328 site ($P_{lacUV5\ 52C}$) to facilitate formation of a stalled transcription elongation complex via
329 nucleotide deprivation. Stalled RNAP acts as a barrier to the replisome in both head-
330 on and co-directional orientations and prevents the formation of full-length replication
331 products (1). Arresting the replisome at this RNAP block resulted in replication
332 products consisting of four truncated leading strands. The strand sizes matched those
333 expected for replisomes moving clockwise or counter-clockwise from *oriC* and
334 encountering $P_{lacUV5\ 52C}$ or the promoters within the *ColE1* plasmid origin of replication
335 (Figure 5A, lane 2 and Figure 5C) (1).
336 Inclusion of UvrD before replication initiation enabled movement of replisomes
337 through stalled RNAP and resulted in a decrease in all four truncated leading strand
338 products and a concomitant increase in production of full-length leading strands
339 (Figure 5A, lane 5 and 5E) (1). Addition of UvrD once the replisome had already
340 encountered the block gave variable results that ranged from an inhibitory to a stronger
341 effect, although differences were not statistically significant at $p<0.05$ (Figure 5A,
342 compare lane 5 with 6, Figure 5E). Similar results were also obtained for Rep (Figure
343 5A, compare lane 3 with 4, Figure 5E). In the absence of replication neither Rep nor
344 UvrD are capable of pushing stalled RNAP from the $P_{lacUV5\ 52C}$ stall site (1). We found
345 that the mGFP tag does not prevent UvrD from dislodging a protein block
346 (Supplementary Figure S14).

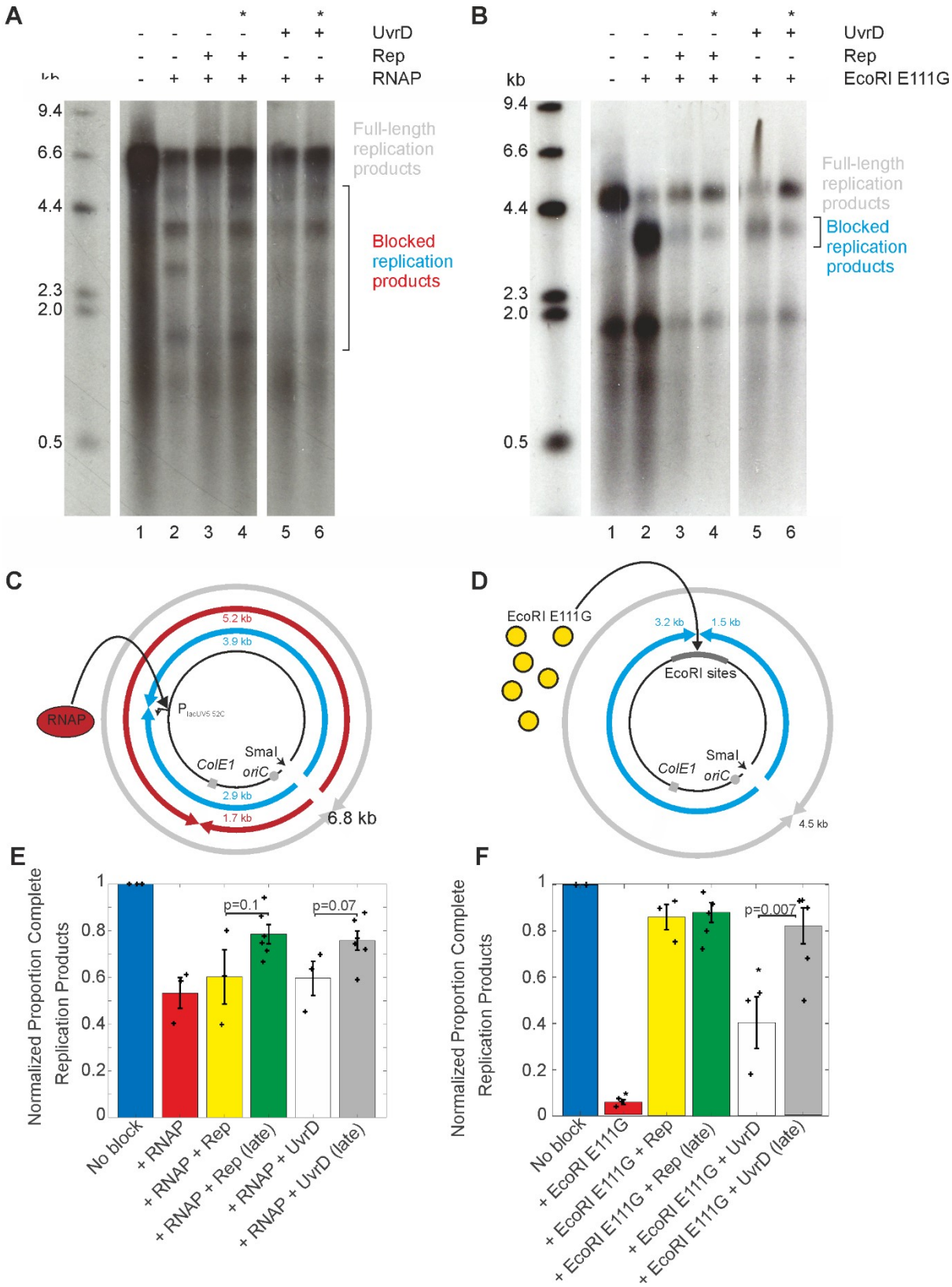

Figure 5: Helicase pre-association affects the promotion of replication fork movement through different nucleoprotein blocks A. Denaturing agarose gel of replication products formed from pPM872 (1) in the absence and presence of RNAP block, Rep and UvrD added pre- and post-collision (*) as indicated. B. Denaturing agarose gel of replication products formed from pPM594 (12) in the absence and presence of EcoRI E111G block, Rep and UvrD added pre- and post-collision (*) as indicated. Truncated leading strand products formed by

354 replisomes originating from *oriC* and colliding with RNAP (C) and EcoRI E111G (D).
355 Quantification of lanes in (A) and (B) from three technical replicates shown in (E) and (F),
356 with standard error in the mean indicated and each replicate result shown as a cross.
357

358 Since UvrD has been shown to interact with RNAP (47–49), we tested whether UvrD-
359 block pre-association is a requirement for its promotion of replication. EcoRI E111G is
360 a mutant restriction enzyme that binds to its recognition sequence but has reduced
361 cleavage activity (96). EcoRI E111G can thus act as an engineered replication fork
362 block that can be overcome by Rep or UvrD helicase activity (12). We tested whether
363 UvrD helicase could promote replication through this barrier when added before or
364 after initiation of replication on a plasmid template with an array of eight EcoRI sites
365 (Figure 5B and D). Adding UvrD post-collision did not impede its promotion of
366 replication; in fact the resolution of these collisions appeared to be more efficient
367 because the proportion of full-length replication products increased (Figure 5B,
368 compare lane 5 and 6, 5F). Quantification of full-length replication products as a
369 proportion of reaction products showed that late UvrD addition increased full-length
370 replication products to 84% (n=6) from 41% (n=3) when UvrD is present before fork
371 collision. This contrasts with the RNAP block results where the UvrD-RNAP interaction
372 (47–50) might be responsible for localising UvrD to the block and facilitating resolution,
373 resulting in no difference when present pre- or post-collision. Similarly, Rep associates
374 directly with the replication fork, also resulting in no difference when present pre- or
375 post-collision, for both blocks. These results suggest that UvrD might recognize stalled
376 replication forks at nucleoprotein blocks using a different mechanism than Rep.
377 Combining these data with the lack of a specific replisome partner and reductions in
378 colocalisation between UvrD and DnaQ fork marker when replication blocks are
379 perturbed *in vivo*, leads us to propose that UvrD is present at the replication fork due
380 to the high frequency of different types of blocks to replication.
381

382 **DISCUSSION**

383 Here, we show that the majority of replisomes are associated with UvrD; but unlike the
384 established Rep association, UvrD has no interaction partner in the replisome. UvrD
385 instead associates with the replisome through the frequent blocks to replication
386 encountered by the fork. Similarly to Rep, *in vitro* evidence suggests UvrD functions
387 poorly as a helicase when monomeric (97). We showed previously that functional Rep
388 foci were hexameric *in vivo* but that this oligomerisation is due to interactions with

389 hexameric DnaB (13). Again, UvrD functions differently and appears to self-associate
390 into tetramers, as evidenced here by tetramer periodicity at and away from the fork
391 (Figure 2 and Supplementary Figure 11) and previous ultracentrifugation experiments
392 *in vitro* (57). It is possible that UvrD may not have evolved to fulfil exactly the same
393 function as Rep. It is common in many enzyme-catalysed reactions that if one enzyme
394 is depleted then another will be available to take its place, but with a reduced catalytic
395 efficiency (98). On initial inspection, this might appear to be the case for Rep and
396 UvrD, in light of the lower efficiency of block resolution for UvrD compared to Rep,
397 noting that deletion of Rep has a profound impact on replication whereas lack of UvrD
398 does not (99). However, we have shown that Rep and UvrD have distinctly different
399 modes of recruitment at a replication block. These differing mechanisms of replication
400 promotion may suggest a model in which these accessory helicases have evolved to
401 fulfil the same overall function (i.e. that of resolving a block to DNA replication) but in
402 different ways. Even with different block removal efficiency, such redundancy may
403 confer an increased level of robustness, helping to ensure that the vital process of
404 DNA replication is carried out correctly by the cell.

405 We used single-molecule microscopy to show that a high proportion of forks,
406 80%, are associated with UvrD *in vivo.* Although the raw imaging data of our Slimfield
407 microscopy is still subject to the optical resolution; the localization tracking algorithms
408 applied can pinpoint fluorescently labelled UvrD to approximately 40 nm lateral
409 precision, smaller than the 50 nm diameter of the replisome machinery itself (69) and
410 equivalent to ~100 bp DNA. Thus, our measurements for colocalisation between UvrD
411 and DnaQ are likely to be good indicators of a real interaction between the replication
412 fork and UvrD. Importantly, the degree of colocalisation we observed is much higher
413 than expectations of random overlap of the optical images of DnaQ-mCherry and
414 mGFP-UvrD.

415 Through SPR, however, we could not find any interaction partner at the
416 replisome apart from Tau. As a control, we tested Tau's interaction with a Rep
417 helicase, and also found a positive interaction. Thus, we conclude that the interaction
418 of UvrD with Tau is likely non-specific and UvrD recruitment to the replisome is
419 mediated by blocks, rather than an interaction partner at the replisome. However, we
420 cannot know the oligomeric state of UvrD on the SPR chip and UvrD's tetrameric form
421 may affect its interactions with replisome components.

422 We probed UvrD's function at the replication fork by perturbing its known DNA
423 repair processing functions, specifically by knocking out *mutS* and *uvrA*, thus blocking
424 mismatch and nucleotide excision repair respectively. We also introduced a mutant
425 RNAP with *rpoB*35* and treated the wild type with rifampicin to reduce the occurrence
426 of transcriptional blocks to translocating replication machinery. Deleting *uvrA* and
427 rifampicin treatment produced clear results, reduced fork colocalization, but deleting
428 *mutS* and introducing the *rpoB*35* mutation did not. However these latter perturbations
429 did result in an identical phenotype of one extra UvrD tetramer per fork. The *rpoB*35*
430 mutation improves cell viability to increased DNA lesions (92). This intriguing link
431 between mutations requires further study, possibly of these dual labelled strains in
432 response to increased DNA lesions. These data support the hypothesis that UvrD is
433 recruited to the replisome by replicative blocks. This is substantiated by the reduced
434 frequency of colocalization observed when mismatch repair and nucleotide excision
435 repair pathways involving UvrD are disrupted. RNA polymerases are the most
436 frequently encountered barrier to replication and we also see a reduction in
437 colocalization when RNA polymerases are removed by the antibiotic.
438 The only function of UvrD we did not probe directly here was its role in RecA-
439 mediated recruitment. We believe the results from a *recA* knockdown would be difficult
440 to interpret due to its pleiotropic effects. RecA is the principal recombinase and
441 induces the complex SOS response resulting in the induction of UvrD expression (100,
442 101). Furthermore, UvrD removes RecA from RecA-DNA complexes, thus functioning
443 as an antirecombinase (102–104). Dissecting these functions of UvrD from other
444 effects that a *recA* mutation may have on the cell would be difficult. Applying the
445 perturbations in combination, i.e. double knockdowns or knockdowns plus rifampicin,
446 would likely lead to confusing results since too many deleterious perturbations may be
447 lethal or change normal cell function too radically to be biologically relevant in the
448 intended way.
449 For the suite of mutant strains investigated we found small but significant
450 changes in colocalisation of UvrD with the replication fork, implying that UvrD is
451 recruited to the replication fork by the frequent blocks to replication it encounters. For
452 example, the UvrD-RNAP interaction could localise UvrD to the vicinity of active
453 transcription machinery (50). Since RNA polymerase is the most common replication
454 block, a secondary consequence would be UvrD-fork colocalisation. This is in contrast
455 to the Rep accessory helicase which has a specific interaction partner in the replisome

456 of the replicative helicase DnaB (89). Recent biochemical findings *in vitro* show that
457 blocks to replication occur very frequently (1)(19)(105), potentially accounting for our
458 finding that UvrD colocalises with the fork more frequently than Rep, despite Rep
459 having a specific interaction partner at the fork.

460 We have shown that replication forks stalled at transcriptional blocks can be
461 rescued by addition of UvrD, prior to or post-stalling. If UvrD is to help perform this
462 function then it must be present during the resolution of collision between the
463 replication and transcription machinery, however, our estimate for dwell time at the
464 fork of just a few milliseconds (compared to seconds for DnaQ (79)) suggests a non-
465 negligible dissociation constant; UvrD is not processive *per se* but rather undergoes
466 rapid turnover at the fork such that there is a high likelihood for UvrD being present at
467 any given time, but not necessarily the same set of molecules. Interestingly we
468 observed a similar dwell time for Rep (13), despite it having a clear association partner
469 in DnaB at the fork. However, using a defective restriction enzyme EcoRI E111G block
470 produced a different effect, with late UvrD addition improving block resolution. This
471 restriction enzyme block is artificial and less biologically relevant but may indicate that
472 the known specific UvrD interaction with RNAP is important. Improved replication
473 resolution with late addition of UvrD is intriguing, implying increased affinity for or
474 activity at pre-stalled replication forks compared to UvrD being present as the fork
475 stalls. Complete understanding requires further study of replication block resolution in
476 different conditions.

477 Our results suggest a model where UvrD diffuses and transiently interacts with
478 DNA at random or through specific interactions such as with RNAP or a specific
479 conformation of the blocked replication fork. At the DNA, UvrD is predominantly
480 tetrameric, either pre-assembling in solution or on the DNA itself. The frequent
481 sampling leads to UvrD often being in the vicinity of the replisome, allowing UvrD to
482 resolve the frequent blocks to replication. It is also possible that certain barriers to
483 replication may be harder for Rep to resolve, and such barriers can possibly be more
484 efficiently removed by UvrD, however, it is still likely to be the case that they do not
485 directly challenge the ability of the cell to replicate the genome in light of *uvrD* deletion
486 still resulting in viable cells. Indeed, UvrD shares a high degree of structural similarity
487 with Rep, although the two proteins differ significantly in their amino acid sequences
488 (31, 106). While Rep is recruited to the fork through specific interactions with DnaB,

489 no such interaction could be identified for UvrD. Stochastic impairment of the ability of
490 Rep to interact with DnaB may necessitate block processing at the fork by UvrD. In
491 summary, our results highlight the contribution of UvrD action to facilitating accurate
492 genome duplication at active replisomes.

493 **Acknowledgments**

494 We thank Maria Chechik for help with mGFP-UvrD purification. We thank Prof. Nigel
495 Savery (University of Bristol) for the gift of the pETDuet-UvrD overexpression plasmid.
496 We thank the Molecular Interactions Laboratory in the Bioscience Technology Facility
497 at the University of York for technical assistance and support. Supported by BBSRC
498 via grants BB/N006453/1 (M.L., P.M.), BB/R001235/1 (M.L., (M.L.,P.M.,A.S.),
499 BB/N014863/1 (M.H.).

500

501 **Author Contributions**

502 Conceptualization: AJMW, AS, PMG, MH, MCL
503 Methodology: AJMW, AS, JALH, AL, CG, PMG, MH, MCL
504 Software: AJMW
505 Investigation: AJMW, AS, JALH, APD, AL, CG, MH
506 Visualization: AJMW, AS, MH
507 Supervision: AJMW, AS, MH, PMG, MCL
508 Writing—original draft: AJMW, AS, MH, MCL
509 Writing—review & editing: AJMW, AS, JALH, AL, PMG, MH, MCL
510

511 **Declaration of interests**

512 The authors declare no competing interests.
513

514 **MATERIALS AND METHODS**

515 **Strain construction**

516 All strains used in this study (listed in full in SI Table S1, with associated plasmids
517 and primers in SI Tables S2 and S3) are derivatives of the laboratory wild type strain
518 TB28. Tagging of *dnaQ-mCherry-<kan>* (C-terminally labelled) is described in (13).

519 *mGFP-uvrD-<kan>* (N-terminally labelled) was amplified from plasmid pAS79 (*uvrD*$^{+}$)
520 with primers oAS145 and oJGB383 having 50 bp homology to either end of the
521 native *uvrD* locus. The resulting PCR product had homology either side such that
522 recombination with the chromosome would result in integration of the PCR product at
523 the native locus under the control of the native promoter. Prior to integration, all PCR
524 products were treated with DpnI, gel purified, and introduced by electroporation into
525 cells expressing the lambda Red genes from the plasmid pKD46 (55). The
526 recombinants were selected for kanamycin resistance and screened for ampicillin
527 sensitivity. The colonies obtained were verified for integration by PCR and
528 sequencing. The *uvrD* recombinants were verified by PCR amplification using
529 primers oPM319 and oPM320, and sequencing using the primers oJGB417,
530 oJGB418, oPM407, oPM409, oPM411, and oMKG71. Where required, the
531 kanamycin resistance gene was removed by expressing Flp recombinase from the
532 plasmid pCP20 (58) to generate kanamycin sensitive strains carrying the fluorescent
533 protein (FP) fusions. Dual labelled strains were created by introducing the kanamycin
534 tagged FP alleles by standard P1 mediated transduction into single labelled strains
535 carrying the required FP allele after removing the linked kanamycin marker.

536 **Determination of cell doubling time**

537 *E. coli* strains were grown overnight in LB medium at 37°C at 200 rpm shaking. The
538 saturated overnight cultures were diluted 100 fold into fresh LB or washed once with
539 1X 56 salts and diluted 100 fold in fresh 1X 56 salts with 0.2% glucose as the carbon
540 source. Aliquots of 100 µl each of the diluted cultures in fresh media were pipetted
541 into individual wells of 96 well clear flat bottom sterile microplates (Corning). The
542 microplates containing the diluted cultures were incubated in a BMG LABTECH
543 SPECTROstar Nano microplate reader at 37°C and the optical density (A_{600}) values
544 were recorded at defined time intervals. The time taken for the optical density values
545 to increase two fold during the exponential growth phase of the culture was taken as
546 the cell doubling time (SI Table S4, Supplementary Figure S1).

547 **Protein Overexpression and Purification**

548 *mGFP-uvrD* was excised from pAS79 using XhoI and SalI and ligated into pET14b
549 cut with XhoI, creating pAS152 encoding N-terminal histidine-tagged mGFP-UvrD.
550 pAS152 was used to overexpress the mGFP-UvrD fusion in Rosetta™

551 2(DE3)/pLysS. The cells were grown in LB medium containing 100 µg/ml ampicillin
552 and 30 µg/ml chloramphenicol at 37ºC and 220 rpm to OD_{600} ~ 0.7. The cultures
553 were then equilibrated to room temperature and overexpression was induced by
554 adding 1 mM IPTG and incubating at 16ºC for 24 hours. Cells from the expressed
555 culture were collected by centrifugation at 4ºC and frozen at -80ºC. The cells were
556 later thawed on ice and resuspended in buffer A (20 mM Tris-Cl pH 8.3, 500 mM
557 NaCl, 5 mM imidazole, 10% glycerol) along with 0.1 mg/ml lysozyme, 1 mM AEBSF,
558 0.7 µg/ml pepstatin, 0.5 µg/ml leupeptin, 2.5 µg/ml DNase I and 20 µg/ml RNase A
559 and incubated on ice for 30 minutes. Brij-58 was then added to a final concentration
560 of 0.1% v/v and incubated on ice for another 20 minutes. The suspension was
561 sonicated and then clarified by centrifugation at 18,000 rpm for 60 minutes at 4ºC in
562 an SS-34 rotor to remove debris. The lysate containing mGFP-UvrD was applied to a
563 5 ml His-trap FF crude column (GE healthcare) and the protein was purified by
564 chromatography on an imidazole gradient in buffer A. Peak fractions were collected
565 and concentrated using a Vivaspin 500 concentrator (30 kDa MWCO) (Sartorius).
566 Samples were then aliquoted and flash frozen in liquid nitrogen before storage at -
567 80ºC. Protein concentration was determined by Bradford's assay.

568 UvrD was purified as previously described (59). Briefly UvrD was overexpressed in
569 BL21-AI from a pETDuet vector, via induction by IPTG and arabinose. UvrD was
570 purified from the soluble cell extract after lysis through the use of affinity (heparin
571 agarose), anion exchange (Q-sepharose), and gel filtration chromatography. Pure
572 UvrD was then stored at -80ºC after dialysis into storage buffer or used immediately
573 in Size Exclusion Chromatography - Multi-Angle Laser Light Scattering (SEC-
574 MALLS) analysis.

575 Biotinylated UvrD and Rep were purified as previously described (60). Briefly, the
576 proteins were overexpressed in a BL21 (DE3) containing pBirAcm, encoding a biotin
577 ligase via induction by IPTG and the addition of biotin to the growth media. The
578 biotinylated proteins were then purified from the soluble cell extracts by ammonium
579 sulphate precipitation, and affinity chromatography (softlink avidin and heparin
580 agarose). Pure proteins were then dialysed into storage buffer overnight and stored
581 at -80°C

582 **Helicase assay**

583 Assays for unwinding of streptavidin-bound forks were performed using a substrate
584 made by annealing oligonucleotides oPM187B20 (5' end labelled with ^{32}P) and
585 oPM188B34. Reactions were performed in 10 µL volumes containing 40 mM HEPES
586 (pH 8); 10 mM DTT; 10 mM magnesium acetate; 2 mM ATP; 0.1 mg ml^{-1} BSA and
587 1 nM forked DNA substrate. Reactions were carried out as described earlier (13, 61).
588 Briefly, the reaction mixture was pre-incubated at 37°C for five minutes with or
589 without 1 µM streptavidin (Sigma-Aldrich), to which helicase (as indicated) and biotin
590 (Sigma-Aldrich) were added to 100 µM (acting as a trap for free streptavidin) and
591 incubated at 37°C for another 10 minutes. Reactions were stopped by addition of 2.5
592 µl of 2.5% SDS, 200 mM EDTA and 10 mg ml^{-1} of proteinase K. Reactions were then
593 analysed by non-denaturing gel electrophoresis on 10% polyacrylamide TBE gels.
594 The quantification of the unwinding and displacement of streptavidin from the fork
595 was carried out as described in (62).

596 **Preparation of cells for microscopy**

597 Cells were grown overnight in LB to saturation. The overnight cultures were
598 inoculated the next day at 1:1000 dilution in 1X 56 salts supplemented with 0.2%
599 glucose as the carbon source. The dilutions were then grown at 30°C to mid-log
600 phase.

601 **Rifampicin treatment**

602 Cells prepared for microscopy were treated with rifampicin at a final concentration of
603 50 µg/mL for 30 minutes at 30°C.

604 **Microscopy and image analysis**

605 Imaging was performed on a bespoke dual-colour single-molecule microscope (13).
606 Excitation from Obis 488 nm and 561 nm wavelength 50mW lasers (run at 20 mW)
607 was reduced to 10 µm at full width half maximum field in the sample plane producing
608 Slimfield illumination (63) producing a mean excitation intensity of ~0.25 mW/μm^2.
609 Lasers were digitally modulated to 5 ms period to produce alternating laser excitation
610 using National Instruments dynamic I/O module NI 9402. Excitation was coupled into
611 a Zeiss microscope body with the sample mounted on a Mad City Labs nanostage.
612 Images were magnified to 80nm/pixel and imaged using an Andor Ixon 128 emCCD
613 camera. Colour channels were split red/green using a bespoke colour splitter

614 consisting of a dual-pass green/red dichroic mirror centred at long-pass wavelength
615 560 nm and emission filters with 25 nm bandwidths centred at 542 nm and 594 nm.

616 Cells were imaged on agarose pads suffused with minimal media as described
617 previously (64). Foci were detected and tracked using previously described bespoke
618 MATLAB software (65). In brief, bright candidate foci were detected in each frame by
619 image transformation and thresholding. A 17x17 pixel region of interest (ROI) is
620 drawn around each candidate and subjected to iterative Gaussian masking (66). Foci
621 were accepted if their signal to noise ratio was above 0.4. Foci in successive frames
622 were linked together into trajectories based on nearest distance, provided it was < 5
623 pixels. Linked foci were accepted as “tracks” nominally if they persist for at least 4
624 consecutive image frames.

625 Characteristic intensity of mGFP or mCherry was determined from the distribution of
626 foci intensity values towards the end of the photobleach confirmed by overtracking
627 foci beyond their bleaching and applying an edge-preserving filter (67, 68) to the raw
628 intensity data to generate individual steps of the characteristic intensity, due to
629 photobleaching (Supplementary Figure S7). This intensity was used to determine the
630 stoichiometry of foci by fitting the first 3 intensity points with a straight line and
631 dividing the intercept by this characteristic intensity. The number of peaks in the
632 Gaussian fits to UvrD was set by running a peak fitting algorithm over the wild type
633 distribution. This number of Gaussians was then used for mutant distributions unless
634 two or more of the Gaussians converged on the same/similar peak value, in which
635 case they were removed. For DnaQ, two peaks were fit as used previously (69).

636 GFP and mCherry images were aligned based on the peak of the 2D cross
637 correlation between their respective brightfield images. Colocalisation between foci
638 and the probability of random colocalisation was determined as described previously
639 (70, 71).

640 The microscopic apparent diffusion coefficients (*D*) were determined by fitting a
641 straight line to the first three mean squared displacements (MSD) values constrained
642 through the equivalent localization precision MSD as determined from the intensity
643 (72, 73). *D* distributions were fit by three Gamma distributions as described
644 previously (74–76). Dwell time was calculated as the number of frames that each

645 trajectory was colocalised with the fork position, as determined by the DnaQ foci
646 detected at time zero.

647 **SEC-MALLS**

648 Size Exclusion Chromatography – Multi-Angle Laser Light Scattering (SEC-MALLS)
649 experiments used Wyatt HELEOS-II multi-angle light scattering and rEX refractive
650 index detectors linked to a Shimadzu HPLC system (SPD-20A UV detector, LC20-
651 AD isocratic pump system, DGU-20A3 degasser and SIL-20A autosampler) with a
652 G.E. Superdex S200 10/300 column at a flow rate of 0.5 mL/min in buffer of 20 mM
653 Tris pH 8.3 (at 4degC) 1 mM EDTA, 1 mm EGTA, 1 mM DTT, 200 mM NaCl, 5%
654 glycerol buffer. Data were analysed using Wyatt Astra 7 software. MWs were
655 estimated using the Zimm fit method with degree 1. A value of 0.182 mL/g was used
656 for protein refractive index increment (dn/dc).

657 **Surface plasmon resonance (SPR)**

658 SPR was performed at 25°C on a BIAcore T200 instrument as in (12). Immobilisation
659 of *E. coli* UvrD and Rep was performed onto streptavidin-coated SA sensor chips
660 whilst the indicated concentrations of Tau and UvrB were passed over in 10 mM
661 HEPES pH 7.4, 3 mM EDTA, 150 mM NaCl, 10 mM $MgCl_2$ and 0.05% Tween 20 at
662 20 µl min^{-1}. This buffer differed from that used in the DNA replication assays to
663 minimise non-specific interactions with the surface-immobilised streptavidin.

664 **Replication assay**

665 Replication assays were carried out using pPM872 as the template for RNAP blocks
666 (1) or pPM594 (12) for EcoRI E111G blocks. Plasmid pPM872 contains $P_{lacUV5\ 52C}$, a
667 strong promoter in which the first 52 nucleotides of the transcript lack cytosine
668 residues and are then followed by four consecutive cytosines. This enables
669 transcription of $P_{lacUV5\ 52C}$ to be stalled by the omission of CTP. Assays were
670 performed in 40 mM HEPES (pH 8); 10 mM DTT; 10 mM magnesium acetate; 2 mM
671 ATP; 0.2 mM GTP, 0.2 mM UTP; 0.04 mM dNTPs; and 0.1 mg/ml BSA. Reactions
672 (15 µl) contained 2 nM plasmid template, 50 nM DNA polymerase III αεθ complex,
673 25 nM τ clamp loader complex, 160 nM DnaB and DnaC monomers, 1 µM SSB, 80
674 nM β clamp, 30 nM HU, 200 nM DnaG, 300 nM DnaA. Helicases were added as
675 indicated. Rep and UvrD used at 200 nM. *E. coli* RNAP holoenzyme from NEB (1

676 U/µl) was used at 1/3 dilution. Dilution was determined empirically to match RNAP
677 replication inhibition levels from (1). EcoRI E111G was purified as in (77) and used
678 at 200 nM. Reactions were assembled on ice and initiated by addition of DnaA and
679 incubation for 4 min at 37°C, followed by addition of 60 units SmaI (Promega) plus
680 0.4 MBq [α^{32}P] dCTP (222 TBq/mmol). Standard reactions with the helicase present
681 in the initial protein mix were carried out at 37°C for 1 minute and then terminated by
682 addition of 1 µl of 0.5 M EDTA. Delayed helicase addition was carried out by adding
683 Rep/UvrD after 1 minute and incubation for a further minute at 37°C before
684 termination with EDTA. Ethanol precipitated replication products were analysed by
685 denaturing agarose gel electrophoresis (0.7% agarose in 2 mM EDTA, 30 mM NaOH
686 for 400 volt hours, standard run was 16 hours at 25 V), phosphorimaging and
687 autoradiography. 5'-labelled HindIII- digested lambda DNA was used as a marker.
688 Gels were quantified using Quantity One® (Bio-Rad) software. Full-length plasmid
689 replication products were quantified as a proportion of summed blocked products
690 and normalised for length (for EcoRI E111G block), or total lane signal (RNAP
691 block).

692

693
694

695

696

697 **REFERENCES**
698

699 1. M. Hawkins, *et al.*, Direct removal of RNA polymerase barriers to replication by
700 accessory replicative helicases. *Nucleic Acids Res.* **47** (2019).
701 2. R. T. Pomerantz, M. O'Donnell, The replisome uses mRNA as a primer after
702 colliding with RNA polymerase. *Nature* **456**, 762–767 (2008).
703 3. H. Merrikh, C. Machón, W. H. Grainger, A. D. Grossman, P. Soultanas, Co-
704 directional replication-transcription conflicts lead to replication restart. *Nature*
705 **470**, 554–7 (2011).
706 4. A. H. Syeda, J. Atkinson, R. G. Lloyd, P. McGlynn, The balance between
707 recombination enzymes and accessory replicative helicases in facilitating
708 genome duplication. *Genes (Basel).* **7** (2016).
709 5. A. Helmrich, M. Ballarino, L. Tora, Collisions between replication and
710 transcription complexes cause common fragile site instability at the longest
711 human genes. *Mol. Cell* **44**, 966–977 (2011).
712 6. Y. Takeuchi, T. Horiuchi, T. Kobayashi, Transcription-dependent
713 recombination and the role of fork collision in yeast rDNA. *Genes Dev.* **17**,
714 1497–1506 (2003).
715 7. A. L. de Septenville, S. Duigou, H. Boubakri, B. Michel, Replication fork
716 reversal after replication-transcription collision. *PLoS Genet.* **8** (2012).
717 8. C. J. Rudolph, A. L. Upton, A. Stockum, C. A. Nieduszynski, R. G. Lloyd,
718 Avoiding chromosome pathology when replication forks collide. *Nature* **500**,
719 608–611 (2013).
720 9. B. Michel, G. Grompone, M. J. Florès, V. Bidnenko, Multiple pathways process
721 stalled replication forks. *Proc. Natl. Acad. Sci. U. S. A.* **101**, 12783–12788
722 (2004).
723 10. E. V. Mirkin, S. M. Mirkin, Mechanisms of transcription-replication collisions in
724 bacteria. *Mol. Cell. Biol.* **25**, 888–895 (2005).
725 11. P. McGlynn, N. J. Savery, M. S. Dillingham, The conflict between DNA
726 replication and transcription. *Mol. Microbiol.* **85**, 12–20 (2012).
727 12. C. P. Guy, *et al.*, Rep provides a second motor at the replisome to promote
728 duplication of protein-bound DNA. *Mol. Cell* **36**, 654–666 (2009).
729 13. A. H. Syeda, *et al.*, Single-molecule live cell imaging of Rep reveals the
730 dynamic interplay between an accessory replicative helicase and the
731 replisome. *Nucleic Acids Res.* **47**, 6287–6298 (2019).
732 14. P. McGlynn, Linking transcription with DNA repair, damage tolerance, and
733 genome duplication. *Proc. Natl. Acad. Sci. U. S. A.* **107**, 15314–15315 (2010).
734 15. D. Dutta, K. Shatalin, V. Epshtein, M. E. Gottesman, E. Nudler, Linking RNA
735 polymerase backtracking to genome instability in E. coli. *Cell* **146**, 533–543
736 (2011).
737 16. D. Duchi, *et al.*, RNA Polymerase Pausing during Initial Transcription. *Mol. Cell*
738 **63**, 939–950 (2016).
739 17. G. Ghosal, J. Chen, DNA damage tolerance: a double-edged sword guarding
740 the genome. *Transl. Cancer Res.* **2**, 107–129 (2013).
741 18. S. Hamperl, M. J. Bocek, J. C. Saldivar, T. Swigut, K. A. Cimprich,
742 Transcription-Replication Conflict Orientation Modulates R-Loop Levels and
743 Activates Distinct DNA Damage Responses. *Cell* **170**, 774-786.e19 (2017).
744 19. K. Hizume, H. Araki, Replication fork pausing at protein barriers on
745 chromosomes. *FEBS Lett.* **593**, 1449–1458 (2019).
746 20. K. K. Myka, M. E. Gottesman, DksA and DNA double-strand break repair.

747 *Curr. Genet.* **65**, 1297–1300 (2019).
748 21. K. K. Myka, *et al.*, Inhibiting translation elongation can aid genome duplication
749 in Escherichia coli. *Nucleic Acids Res.* **45**, 2571–2584 (2017).
750 22. S. M. Mangiameli, C. N. Merrikh, P. A. Wiggins, H. Merrikh, Transcription leads
751 to pervasive replisome instability in bacteria. *Elife* **6** (2017).
752 23. V. Kamarthapu, *et al.*, ppGpp couples transcription to DNA repair in E. coli.
753 *Science* **352**, 993–996 (2016).
754 24. B. J. Brewer, When polymerases collide: replication and the transcriptional
755 organization of the E. coli chromosome. *Cell* **53**, 679–686 (1988).
756 25. A. Srivatsan, A. Tehranchi, D. M. MacAlpine, J. D. Wang, Co-orientation of
757 replication and transcription preserves genome integrity. *PLoS Genet.* **6**
758 (2010).
759 26. B. Liu, B. M. Alberts, Head-on collision between a DNA replication apparatus
760 and RNA polymerase transcription complex. *Science* **267**, 1131–1137 (1995).
761 27. J. D. Wang, M. B. Berkmen, A. D. Grossman, Genome-wide coorientation of
762 replication and transcription reduces adverse effects on replication in Bacillus
763 subtilis. *Proc. Natl. Acad. Sci. U. S. A.* **104**, 5608–5613 (2007).
764 28. T. S. Sankar, B. D. Wastuwidyaningtyas, Y. Dong, S. A. Lewis, J. D. Wang,
765 The nature of mutations induced by replication–transcription collisions. *Nature*
766 **535**, 178–181 (2016).
767 29. D. Ivanova, *et al.*, Shaping the landscape of the Escherichia coli chromosome:
768 replication-transcription encounters in cells with an ectopic replication origin.
769 *Nucleic Acids Res.* **43**, 7865–7877 (2015).
770 30. A. Helmrich, M. Ballarino, E. Nudler, L. Tora, Transcription-replication
771 encounters, consequences and genomic instability. *Nat. Struct. Mol. Biol.* **20**,
772 412–418 (2013).
773 31. J. G. Brüning, J. L. Howard, P. McGlynn, Accessory replicative helicases and
774 the replication of protein-bound DNA. *J. Mol. Biol.* **426**, 3917–3928 (2014).
775 32. K. R. McDonald, *et al.*, Pfh1 Is an Accessory Replicative Helicase that
776 Interacts with the Replisome to Facilitate Fork Progression and Preserve
777 Genome Integrity. *PLoS Genet.* **12** (2016).
778 33. J. E. Sokoloski, A. G. Kozlov, R. Galletto, T. M. Lohman, Chemo-mechanical
779 pushing of proteins along single-stranded DNA. *Proc. Natl. Acad. Sci. U. S. A.*
780 **113**, 6194–6199 (2016).
781 34. G. D. Schauer, *et al.*, Replisome bypass of a protein-based R-loop block by
782 Pif1. *Proc. Natl. Acad. Sci. U. S. A.* **117**, 30354–30361 (2020).
783 35. M. K. Gupta, *et al.*, Protein-DNA complexes are the primary sources of
784 replication fork pausing in Escherichia coli. *Proc. Natl. Acad. Sci. U. S. A.* **110**,
785 7252–7257 (2013).
786 36. H. Boubakri, A. L. De Septenville, E. Viguera, B. Michel, The helicases DinG,
787 Rep and UvrD cooperate to promote replication across transcription units in
788 vivo. *EMBO J.* **29**, 145–157 (2010).
789 37. X. Liu, J. X. Seet, Y. Shi, P. R. Bianco, Rep and UvrD Antagonize One Another
790 at Stalled Replication Forks and This Is Exacerbated by SSB. *ACS Omega* **4**,
791 5180–5196 (2019).
792 38. O. Adebali, Y. Y. Chiou, J. Hu, A. Sancar, C. P. Selby, Genome-wide
793 transcription-coupled repair in Escherichia coli is mediated by the Mfd
794 translocase. *Proc. Natl. Acad. Sci. U. S. A.* **114**, E2116–E2125 (2017).
795 39. N. Kang, E. Choi, S. G. Kim, J. Hwang, Inhibitory effect of UvrD and DinG on
796 the replication of ColE1-derived plasmids in Escherichia coli. *Plasmid* **81**, 32–

797 41 (2015).
798 40. V. Epshtein, UvrD helicase: an old dog with a new trick: how one step
799 backward leads to many steps forward. *Bioessays* **37**, 12–19 (2015).
800 41. P. R. Caron, S. R. Kushner, L. Grossman, Involvement of helicase II (uvrD
801 gene product) and DNA polymerase I in excision mediated by the uvrABC
802 protein complex. *Proc. Natl. Acad. Sci. U. S. A.* **82**, 4925–4929 (1985).
803 42. B. Van Houten. Nucleotide excision repair in Escherichia coli. *Microbiol. Rev.*
804 **54**, 18–51 (1990).
805 43. A. L. Lu, S. Clark, P. Modrich, Methyl-directed repair of DNA base-pair
806 mismatches in vitro. *Proc. Natl. Acad. Sci. U. S. A.* **80**, 4639–4643 (1983).
807 44. S. W. Matson, A. B. Robertson, The UvrD helicase and its modulation by the
808 mismatch repair protein MutL. *Nucleic Acids Res.* **34**, 4089–4097 (2006).
809 45. L. Manelyte, *et al.*, The unstructured C-terminal extension of UvrD interacts
810 with UvrB, but is dispensable for nucleotide excision repair. *DNA Repair*
811 *(Amst).* **8**, 1300–1310 (2009).
812 46. A. B. Robertson, S. R. Pattishall, E. A. Gibbons, S. W. Matson, MutL-catalyzed
813 ATP hydrolysis is required at a post-UvrD loading step in methyl-directed
814 mismatch repair. *J. Biol. Chem.* **281**, 19949–19959 (2006).
815 47. E. J. Gwynn, *et al.*, The conserved C-terminus of the PcrA/UvrD helicase
816 interacts directly with RNA polymerase. *PLoS One* **8** (2013).
817 48. K. Sanders, *et al.*, The structure and function of an RNA polymerase
818 interaction domain in the PcrA/UvrD helicase. *Nucleic Acids Res.* **45**, 3875–
819 3887 (2017).
820 49. V. Epshtein, *et al.*, UvrD facilitates DNA repair by pulling RNA polymerase
821 backwards. *Nature* **505**, 372–377 (2014).
822 50. B. K. Bharati, *et al.*, Crucial role and mechanism of transcription-coupled DNA
823 repair in bacteria. *Nature* **604**, 152–159 (2022).
824 51. B. Martinez, B. K. Bharati, V. Epshtein, E. Nudler, Pervasive Transcription-
825 coupled DNA repair in E. coli. *Nat. Commun.* **13** (2022).
826 52. N. M. Haines, Y. I. T. Kim, A. J. Smith, N. J. Savery, Stalled transcription
827 complexes promote DNA repair at a distance. *Proc. Natl. Acad. Sci. U. S. A.*
828 **111**, 4037–4042 (2014).
829 53. A. J. Smith, N. J. Savery, Effects of the bacterial transcription-repair coupling
830 factor during transcription of DNA containing non-bulky lesions. *DNA Repair*
831 *(Amst).* **7**, 1670–1679 (2008).
832 54. A. J. Smith, N. J. Savery, RNA polymerase mutants defective in the initiation of
833 transcription-coupled DNA repair. *Nucleic Acids Res.* **33**, 755–764 (2005).
834 55. J. Atkinson, *et al.*, Stimulation of UvrD helicase by UvrAB. *J. Biol. Chem.* **284**,
835 9612–9623 (2009).
836 56. R. P. Wong, N. García-Rodríguez, N. Zilio, M. Hanulová, H. D. Ulrich,
837 Processing of DNA Polymerase-Blocking Lesions during Genome Replication
838 Is Spatially and Temporally Segregated from Replication Forks. *Mol. Cell* **77**,
839 3-16.e4 (2020).
840 57. N. K. Maluf, T. M. Lohman, Self-association equilibria of Escherichia coli UvrD
841 helicase studied by analytical ultracentrifugation. *J. Mol. Biol.* **325**, 889–912
842 (2003).
843 58. K. A. Datsenko, B. L. Wanner, One-step inactivation of chromosomal genes in
844 Escherichia coli K-12 using PCR products. *Proc. Natl. Acad. Sci. U. S. A.* **97**,
845 6640–6645 (2000).
846 59. J. Atkinson, *et al.*, Stimulation of UvrD helicase by UvrAB. *J. Biol. Chem.* **284**,

847 9612–9623 (2009).
848 60. C. P. Guy, *et al.*, Rep provides a second motor at the replisome to promote
849 duplication of protein-bound DNA. *Mol. Cell* **36**, 654–666 (2009).
850 61. J. G. Brüning, J. A. L. Howard, K. K. Myka, M. S. Dillingham, P. McGlynn, The
851 2B subdomain of Rep helicase links translocation along DNA with protein
852 displacement. *Nucleic Acids Res.* **46**, 8917–8925 (2018).
853 62. J. G. Brüning, J. A. L. Howard, P. McGlynn, Use of streptavidin bound to
854 biotinylated DNA structures as model substrates for analysis of nucleoprotein
855 complex disruption by helicases. *Methods* **108**, 48–55 (2016).
856 63. M. Plank, G. H. Wadhams, M. C. Leake, Millisecond timescale slimfield
857 imaging and automated quantification of single fluorescent protein molecules
858 for use in probing complex biological processes. *Integr. Biol.* **1**, 602–612
859 (2009).
860 64. A. J. M. Wollman, A. H. Syeda, P. McGlynn, M. C. Leake, Single-Molecule
861 Observation of DNA Replication Repair Pathways in E. coli. *Adv. Exp. Med.*
862 *Biol.* **915**, 5–16 (2016).
863 65. H. Miller, *et al.*, Superresolution imaging of single DNA molecules using
864 stochastic photoblinking of minor groove and intercalating dyes. *Methods* **88**,
865 81–8 (2015).
866 66. M. C. Leake, *et al.*, Stoichiometry and turnover in single, functioning
867 membrane protein complexes. *Nature* **443**, 355–358 (2006).
868 67. M. C. Leake, D. Wilson, B. Bullard, R. M. Simmons, The elasticity of single
869 kettin molecules using a two-bead laser-tweezers assay. *FEBS Lett.* **535**, 55–
870 60 (2003).
871 68. M. C. Leake, D. Wilson, M. Gautel, R. M. Simmons, The elasticity of single titin
872 molecules using a two-bead optical tweezers assay. *Biophys. J.* **87**, 1112–35
873 (2004).
874 69. R. Reyes-Lamothe, D. J. Sherratt, M. C. Leake, Stoichiometry and architecture
875 of active DNA replication machinery in Escherichia coli. *Science* **328**, 498–501
876 (2010).
877 70. I. Llorente-Garcia, *et al.*, Single-molecule in vivo imaging of bacterial
878 respiratory complexes indicates delocalized oxidative phosphorylation.
879 *Biochim. Biophys. Acta* **1837**, 811–24 (2014).
880 71. A. J. M. Wollman, *et al.*, Critical roles for EGFR and EGFR-HER2 clusters in
881 EGF binding of SW620 human carcinoma cells. *J. R. Soc. Interface* **19** (2022).
882 72. A. J. M. Wollman, M. C. Leake, Millisecond single-molecule localization
883 microscopy combined with convolution analysis and automated image
884 segmentation to determine protein concentrations in complexly structured,
885 functional cells, one cell at a time. *Faraday Discuss.* **184**, 401–24 (2015).
886 73. M. C. Leake, *et al.*, Variable stoichiometry of the TatA component of the twin-
887 arginine protein transport system observed by in vivo single-molecule imaging.
888 *Proc. Natl. Acad. Sci. U. S. A.* **105**, 15376–81 (2008).
889 74. H. Miller, *et al.*, High-Speed Single-Molecule Tracking of CXCL13 in the B-
890 Follicle. *Front. Immunol.* **9**, 1073 (2018).
891 75. J. Cosgrove, *et al.*, B cell zone reticular cell microenvironments shape CXCL13
892 gradient formation. *Nat. Commun.* **11** (2020).
893 76. X. Jin, *et al.*, Membraneless organelles formed by liquid-liquid phase
894 separation increase bacterial fitness. *Sci. Adv.* **7** (2021).
895 77. S.-C. Chengs, R. Kim, K. Kings, S.-H. Kim, P. Modrich, Isolation of Gram
896 Quantities of EcoRI Restriction and Modification Enzymes from an

897 Overproducing Strain. *J. Biol. Chem.* **259**, 11571–11575 (1984).
898 78. A. Badrinarayanan, R. Reyes-Lamothe, S. Uphoff, M. C. Leake, D. J. Sherratt,
899 In vivo architecture and action of bacterial structural maintenance of
900 chromosome proteins. *Science* **338**, 528–31 (2012).
901 79. T. R. Beattie, *et al.*, Frequent exchange of the DNA polymerase during
902 bacterial chromosome replication. *Elife* **6**, e21763 (2017).
903 80. R. Reyes-Lamothe, C. Possoz, O. Danilova, D. J. Sherratt, Independent
904 positioning and action of Escherichia coli replisomes in live cells. *Cell* **133**, 90–
905 102 (2008).
906 81. A. L. Payne-Dwyer, A. H. Syeda, J. W. Shepherd, L. Frame, M. C. Leake,
907 RecA and RecB: probing complexes of DNA repair proteins with mitomycin C
908 in live Escherichia coli with single-molecule sensitivity. *bioRxiv*,
909 2021.10.04.463068 (2021).
910 82. D. A. Zacharias, J. D. Violin, A. C. Newton, R. Y. Tsien, Partitioning of lipid-
911 modified monomeric GFPs into membrane microdomains of live cells. *Science*
912 **296**, 913–916 (2002).
913 83. N. K. Maluf, C. J. Fischer, T. M. Lohman, A Dimer of Escherichia coli UvrD is
914 the active form of the helicase in vitro. *J. Mol. Biol.* **325**, 913–935 (2003).
915 84. H. Yokota, Y. A. Chujo, Y. Harada, Single-molecule imaging of the oligomer
916 formation of the nonhexameric Escherichia coli UvrD helicase. *Biophys. J.* **104**,
917 924–933 (2013).
918 85. H. Yokota, Quantitative and kinetic single-molecule analysis of DNA unwinding
919 by Escherichia coli UvrD helicase. *Biophys. physicobiology* **19**, n/a (2022).
920 86. H. M. Arthur, P. B. Eastlake, Transcriptional control of the uvrD gene of
921 Escherichia coli. *Gene* **25**, 309–316 (1983).
922 87. Y. Taniguchi, *et al.*, Quantifying E. coli proteome and transcriptome with
923 single-molecule sensitivity in single cells. *Science* **329**, 533–8 (2010).
924 88. G. W. Li, D. Burkhardt, C. Gross, J. S. Weissman, Quantifying absolute protein
925 synthesis rates reveals principles underlying allocation of cellular resources.
926 *Cell* **157**, 624–635 (2014).
927 89. J. Atkinson, M. K. Gupta, P. McGlynn, Interaction of Rep and DnaB on DNA.
928 *Nucleic Acids Res.* **39**, 1351–1359 (2011).
929 90. S. V. Rajagopala, *et al.*, The binary protein-protein interaction landscape of
930 Escherichia coli. *Nat. Biotechnol. 2014 323* **32**, 285–290 (2014).
931 91. D. K. Orrens, C. P. Selbys, J. E. Hearst, A. Sancars, Post-incision Steps of
932 Nucleotide Excision Repair in Escherichia coli DISASSEMBLY OF THE
933 UvrBC-DNA COMPLEX BY HELICASE I1 AND DNA POLYMERASE I*. *J.*
934 *Biol. Chem.* **267**, 780–788 (1992).
935 92. P. McGlynn, R. G. Lloyd, Modulation of RNA polymerase by (p)ppGpp reveals
936 a RecG-dependent mechanism for replication fork progression. *Cell* **101**, 35–
937 45 (2000).
938 93. Y. N. Zhou, D. J. Jin, The rpoB mutants destabilizing initiation complexes at
939 stringently controlled promoters behave like “stringent” RNA polymerases in
940 Escherichia coli. *Proc. Natl. Acad. Sci. U. S. A.* **95**, 2908–2913 (1998).
941 94. E. A. Campbell, *et al.*, Structural mechanism for rifampicin inhibition of
942 bacterial rna polymerase. *Cell* **104**, 901–912 (2001).
943 95. M. Stracy, *et al.*, Live-cell superresolution microscopy reveals the organization
944 of RNA polymerase in the bacterial nucleoid. *Proc. Natl. Acad. Sci. U. S. A.*
945 **112**, E4390-9 (2015).
946 96. K. King, S. J. Benkovics, P. Modrich, Glu-11 1 Is Required for Activation of the

947 DNA Cleavage Center of EcoRI Endonuclease*. *J. Biol. Chem.* **264**, 11807–
948 11815 (1989).
949 97. B. Nguyen, Y. Ordabayev, J. E. Sokoloski, E. Weiland, T. M. Lohman, Large
950 domain movements upon UvrD dimerization and helicase activation. *Proc.*
951 *Natl. Acad. Sci.* **114**, 12178–12183 (2017).
952 98. A. Wagner, Robustness against mutations in genetic networks of yeast. *Nat.*
953 *Genet. 2000 244* **24**, 355–361 (2000).
954 99. J. Atkinson, *et al.*, Localization of an accessory helicase at the replisome is
955 critical in sustaining efficient genome duplication. *Nucleic Acids Res.* **39**, 949–
956 957 (2011).
957 100. S. C. Massoni, S. J. Sandler, Specificity in suppression of SOS expression by
958 recA4162 and uvrD303. *DNA Repair (Amst).* **12**, 1072–1080 (2013).
959 101. K. H. Maslowska, K. Makiela-Dzbenska, I. J. Fijalkowska, The SOS system: A
960 complex and tightly regulated response to DNA damage. *Environ. Mol.*
961 *Mutagen.* **60**, 368–384 (2019).
962 102. R. C. Centore, S. J. Sandler, UvrD limits the number and intensities of RecA-
963 green fluorescent protein structures in Escherichia coli K-12. *J. Bacteriol.* **189**,
964 2915–2920 (2007).
965 103. V. Petrova, *et al.*, Active displacement of RecA filaments by UvrD translocase
966 activity. *Nucleic Acids Res.* **43**, 4133–4149 (2015).
967 104. M. M. Cox, Regulation of bacterial RecA protein function. *Crit. Rev. Biochem.*
968 *Mol. Biol.* **42**, 41–63 (2007).
969 105. N. Raghunathan, S. Goswami, J. K. Leela, A. Pandiyan, J. Gowrishankar, A
970 new role for Escherichia coli Dam DNA methylase in prevention of aberrant
971 chromosomal replication. *Nucleic Acids Res.* **47**, 5698–5711 (2019).
972 106. H. Yokota, Roles of the C-Terminal Amino Acids of Non-Hexameric Helicases:
973 Insights from Escherichia coli UvrD. *Int. J. Mol. Sci.* **22**, 1–19 (2021).
974
975
976

Supplementary Information

Tetrameric UvrD helicase is located at the *E. coli* replisome due to frequent replication blocks

Adam J. M Wollman[1,2,3,], Aisha H. Syeda[1,2], Jamieson A. L. Howard[1,2], Alex Payne-Dwyer[1,2], Andrew Leech[4] , Colin Guy[5, 6], Peter McGlynn[2,6], Michelle Hawkins[2] and Mark C. Leake[1,2]

The authors wish it to be known that, in their opinion, the first two authors should be regarded as joint First Authors

[1] School of Physics, Engineering and Technology, University of York, York YO10 5DD, United Kingdom.

[2] Department of Biology, University of York, York YO10 5DD, United Kingdom.

[3] Current address: Biosciences Institute, Newcastle University, NE1 7RU, United Kingdom.

[4] Bioscience Technology Facility, Department of Biology, University of York, York YO10 5DD, United Kingdom

[5] Current address: Covance Laboratories Ltd., Otley Road, Harrogate, HG3 1PY, United Kingdom

[6] Previous address: School of Medical Sciences, Institute of Medical Sciences, University of Aberdeen, Foresterhill, Aberdeen AB25 2ZD, United Kingdom

* To whom correspondence should be addressed. To whom correspondence should be addressed. Tel: +44 (0)1904322697. Email: mark.leake@york.ac.uk

Present Address: School of Physics, Engineering and Technology, and Department of Biology, University of York, York YO10 5DD, United Kingdom

1001 **Supplementary Tables**

1002 **Table S1 Strains used in this study**

Strain	Relevant genotype	Source or derivation
BW25113 derivatives:		
BW25113	*rrnB ΔlacZ4787 hsdR514 Δ(araBAD)567 Δ(rhaBAD)568 rph-1*	(1)
JW2703	*ΔmutS::<kan>*	(1)
JW3786	*ΔuvrD::<kan>*	(1)
JW4019	*ΔuvrA::<kan>*	(1)
MG1655 derivatives:		
TB12	*ΔlacIZYA::<kan>*	
TB28	*ΔlacIZYA*	(2, 3)
TB28 derivatives		
N6577	*ΔlacIZYA Δrep::cat*	(4)
N6661	*ΔlacIZYA::<> Δrep::dhfr* / pAM407 (*uvrD*$^+$ *lacZ*$^+$, a pRC7 derivative)	(4)
N6661	*ΔlacIZYA::<> Δrep::dhfr* / pAM407 (*uvrD*$^+$ *lacZ*$^+$, a pRC7 derivative)	(4)
N6644	*ΔlacIZYA::<> uvrD::dhfr Δrep::cat* / pAM407 (*uvrD*$^+$ *lacZ*$^+$, a pRC7 derivative)	(4)
JGB166	*ΔuvrD* / pKD46	JW3786 transformed with pKD46
AS97	TB28/pKD46	(5)
AS446	*dnaQ-mCherry-<kan>*	
AS448	*dnaQ-mCherry-<>*	(5)
AS512	*mGFP-uvrD-<kan>*	*mGFP-uvrD-<kan>* recombineered into JGB166
AS517	*ΔlacIZYA::<> Δrep::cat mGFP-uvrD-<kan>* / pAM407 (*uvrD*$^+$ *lacZ*$^+$, a pRC7 derivative)	N6661 X P1(AS512)
AS564	*dnaQ-mCherry-<kan> rpoB*35*	PM486 X P1(AS446)
AS571	*dnaQ-mCherry-<> rpoB*35*	AS564 to km^S with pCP20
AS580	*dnaQ-mCherry-<> mGFP-uvrD-<kan>*	AS448 X P1(AS512)
AS582	*dnaQ-mCherry-<> mGFP-uvrD-<kan> rpoB*35*	AS571 X P1(AS512)
AS590	*dnaQ-mCherry-<> mGFP-uvrD-<kan> Δrep::cat*	AS580 X P1(N6577)
AS650	*dnaQ-mCherry-<> mGFP-uvrD-<>*	AS580 to km^S with pCP20
AS656	*dnaQ-mCherry-<> mGFP-uvrD-<> ΔuvrA::<kan>*	AS650 X P1(JW4019)
AS658	*dnaQ-mCherry-<> mGFP-uvrD-<> ΔmutS::<kan>*	AS650 X P1(JW2703)

1003

1004

1005 **Table S2 Plasmids used in this study**

Plasmid	Description	Antibiotic	Reference
pCP20	Yeast Flp recominase expression plasmid	Amp	(6)
pKD46	λ Red recombinase expression plasmid	Amp	(6)
pAS79	pUC18 *mGFP-uvrD-<kan>*	Amp, kan	This study
pAS152	pET14b-mGFP uvrD	Amp	This study

1006
1007

1008 **Table S3 Oligonucleotides used in this study**

Primer	Sequence (5' - 3')
oJGB383	TGAATGATTTTTTAGGCCAAATAAGGTGCGCAGCACCGCATCCGGCAACGCATATGAATATCCTCCTTAG
oJGB417	TACAAGACACGTGCTGAAGTC
oJGB418	TGCTAGTTGAACGCTTCCATC
oMKG71	CGGTGCCCTGAATGAACTGC
oPM319	CTTGTTGGATCAGACCGGAAAATG
oPM320	TGGCAACGCTATCCTTTTGTCA
oPM407	GCGGCAGGCAATGTGGTA
oPM409	CCTTTGAGCGTGTGGTGA
oPM411	CAGCGGCTACAAGCTCGG
oPM187B20	GTCGGATCCTCTAGACAGC(BiodT)CCATGATCACTGGCACTGGTAGAATTCGGC
oPM188B34	AACGTCATAGACGATTACATTGCTACATGGAGC(BiodT)GTCTAGAGGATCCGAC
oAS84	CCCGTCTCGATCTGGTGCAG
oAS85	TTGCTGCAAAAATCGCCCAAG
oAS132	CCCGTCTCGATCTGGTGCAGAAGAAAGGCGGAAGTTGCCTCTGGCGAGCAGGCTGGCTCCGCTGCTGG
oAS133	TTGCTGCAAAAATCGCCCAAGTCGCTATTTTTAGCGCCTTTCACAGGTATCATATGAATATCCTCCTTAG
oAS145	AGGGCGTTGCGCTTCTCCGCCCAACCTATTTTTACGCGGCGGTGCCAATGAGTAAAGGAGAAGAACTT

1009

1010

1011 **Table S4 Cell doubling times of labelled strains.** Values expressed are the means of three
1012 independent replicates, with standard deviation and standard errors indicated.

Strain (Relevant genotype)	LB medium			Minimal medium		
	Mean doubling time (min)	SD (min)	SEM (min)	Mean doubling time (min)	SD (min)	SEM (min)
WT	23.72	1.11	0.64	62.80	17.06	9.85
dnaQ-mCherry	26.85	0.91	0.52	62.22	18.63	10.76
mGFP-uvrD	24.79	0.37	0.22	59.45	1.80	1.04
dnaQ-mCherry mGFP-uvrD	25.27	1.51	0.87	71.03	7.59	4.38
ΔmutS	24.59	0.55	0.32	107.91	13.96	8.06
ΔuvrA	27.99	0.23	0.13	92.25	5.86	3.38
*ΔrpoB*35*	33.98	0.17	0.10	83.11	30.83	17.80
Δrep	24.30	2.03	1.17	62.74	1.20	0.70
dnaQ-mCherry mGFP-uvrD ΔmutS	26.85	0.68	0.39	110.84	34.91	20.16
dnaQ-mCherry mGFP-uvrD ΔuvrA	24.13	0.56	0.33	91.80	5.18	2.99
*dnaQ-mCherry mGFP-uvrD ΔrpoB*35*	32.81	0.70	0.40	99.11	78.68	45.42
dnaQ-mCherry mGFP-uvrD Δrep	26.54	1.90	1.10	62.17	2.98	1.72

1013
1014
1015
1016
1017

1018

1019 **Supplementary figures**

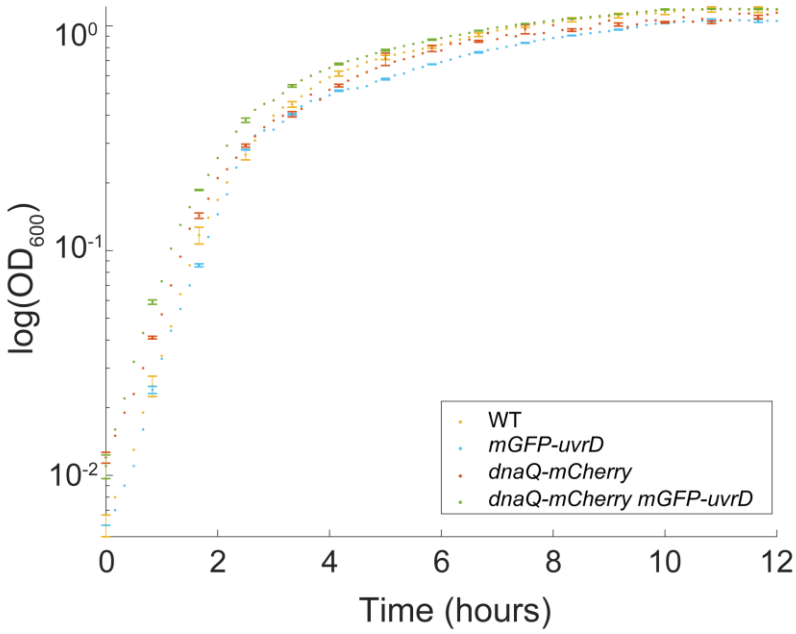

1020

1021

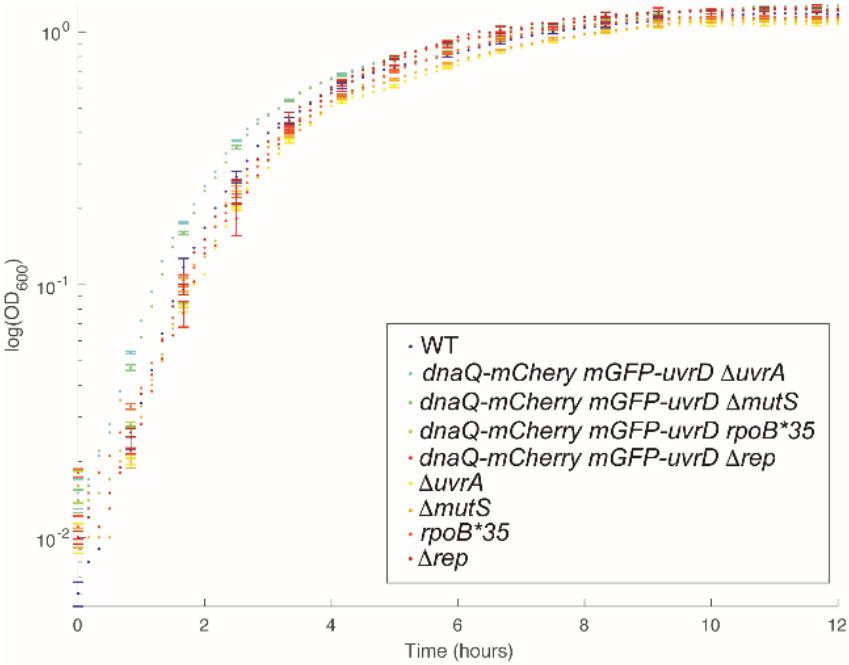

1022

1023 **Supplementary Figure S1. Growth curves in LB medium.** Cultures were grown in LB as
1024 described in the text. The OD_{600} values are plotted on a log scale on the vertical axis with a
1025 linear scale of time in hours on the horizontal axis. The genotypes of the strains are indicated
1026 in boxes within the figures. SD error bars (shown just on every 5th consecutive point for clarity
1027 here), taken from N=3 replicate cultures. Plots in panel A are growth curves of single and dual
1028 labelled wild-type strains, while those in panel B are dual labelled and unlabelled mutant
1029 strains. The unlabelled wild-type strain is included in all panels as a reference.

1030

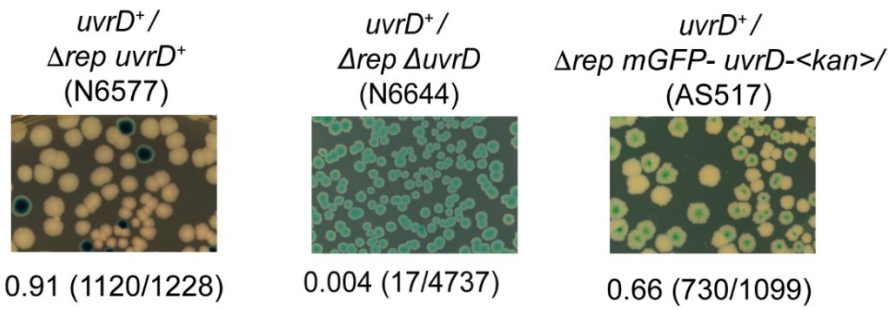

1031

1032 **Supplementary Figure S2: Testing of mGFP-UvrD fusions for retention of function.** We
1033 transformed the strain carrying a chromosomal *mGFP-uvrD* allele with a derivative of pRC7
1034 carrying a wild-type *uvrD* allele (pPM407), which is an unstable low copy plasmid that also
1035 carries the *lacZYA* genes (3). Presence of this plasmid confers blue colour to the colonies on
1036 plates containing Xgal when strains are chromosomally deleted for the *lac* operon. In rapidly
1037 growing cells, cells require either *rep* or *uvrD* for viability, and the loss of both is lethal (4, 7).
1038 Thus, *Δrep* cells with a functional *uvrD* allele are viable and can lose pRC7*uvrD*, evidenced
1039 by appearance of white colonies on LB Xgal IPTG plates, but cells lacking *uvrD* function
1040 cannot survive upon loss of the plasmid resulting in recovery of only blue colonies. The *Δrep*
1041 *mGFP-uvrD* cells produced white colonies on Xgal media, indicating that the *mGFP-uvrD*
1042 fusion is functional.
1043

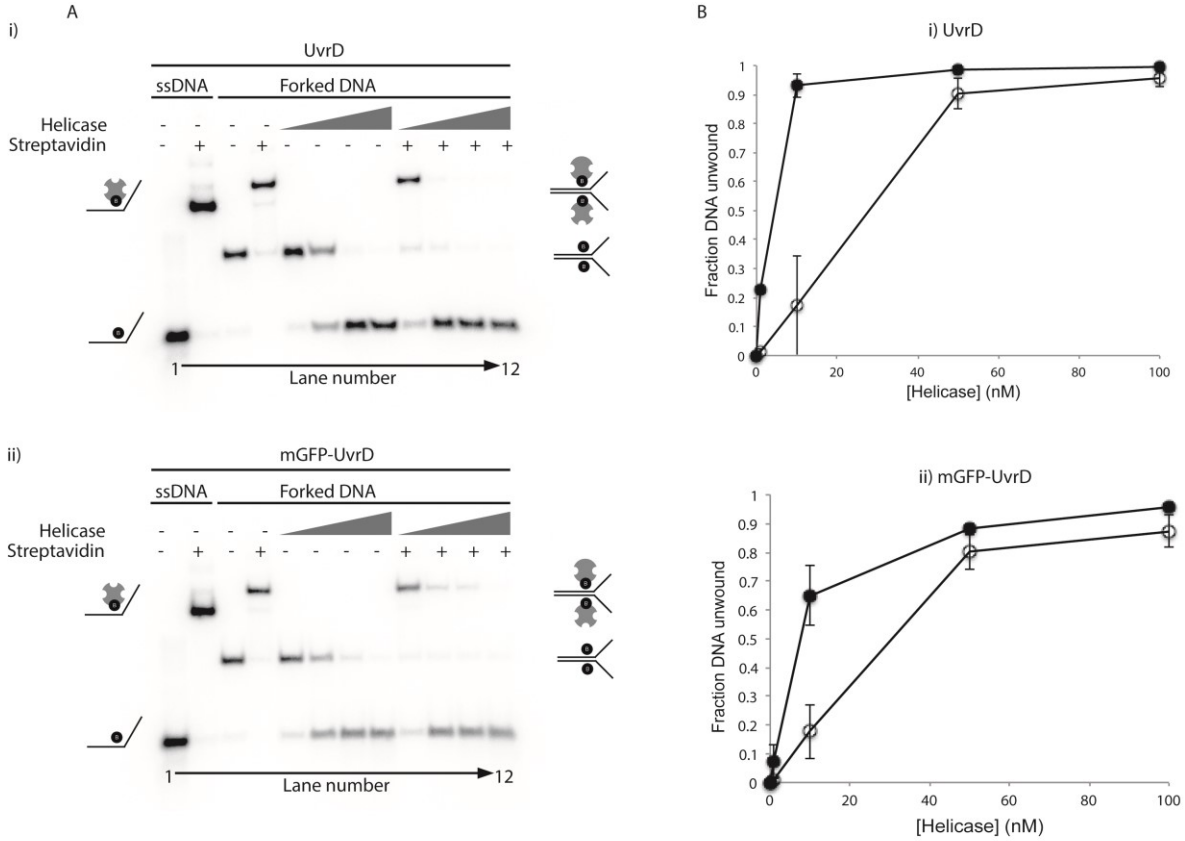

Supplementary Figure S3: mGFP-UvrD fusion is functional *in vitro*. (A) Representative native polyacrylamide TBE gels showing (i) UvrD and (ii) mGFP-UvrD unwinding of forked DNA containing biotin on both strands within the duplex region (8, 9). Lanes 1-4 contain markers indicating the position of single stranded or forked DNA +/- streptavidin as indicated. Lanes 5-12 contain the products of unwinding the forked DNA +/- streptavidin by the indicated helicase at 1, 10, 50 and 100 nM. (B) Quantification of the unwinding of the forked substrate in the absence of (open circles) and presence of (closed circles) streptavidin by the indicated helicases. Data points shown are averages of band intensities (taken from two gels in UvrD and four gels in mGFP-UvrD) with standard errors indicated by bars on the points.

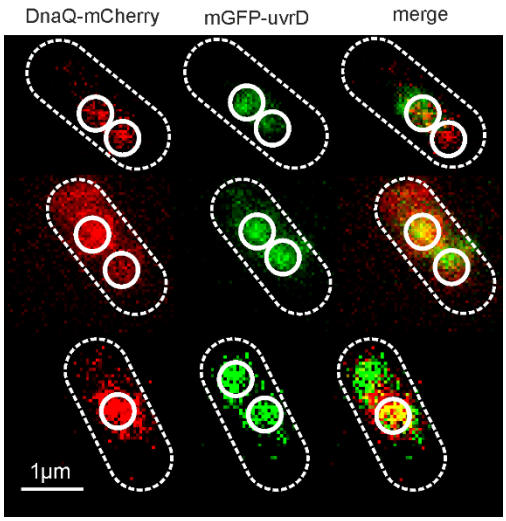

1054

1055 **Supplementary Figure S4:** Dual colour Slimfield images of mGFP-UvrD:DnaQ-mCherry,
1056 scale bar 1 micron. Segmented outlines of cell bodies (white dash) and detected foci (white
1057 circles) indicated.

1058

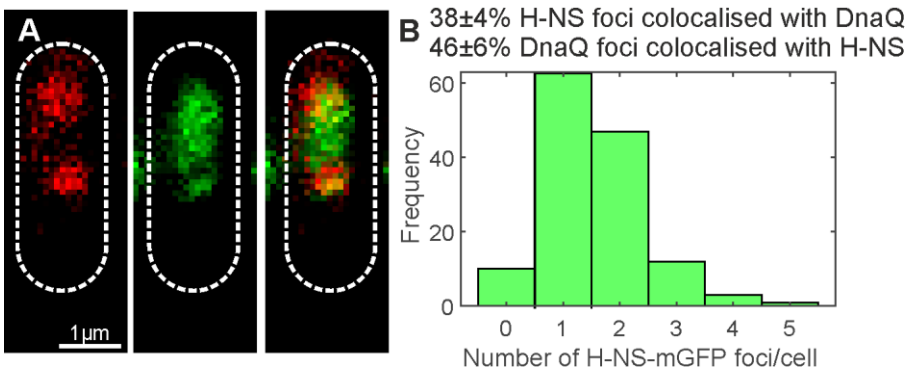

Supplementary Figure S5: (A) Dual colour Slimfield images of H-NS-mGFP-:DnaQ-mCherry, scale bar 1 micron. Segmented outlines of cell bodies indicated (white dash). (B) Histogram showing the number of H-NS foci detected per cell, SD errors.

1064

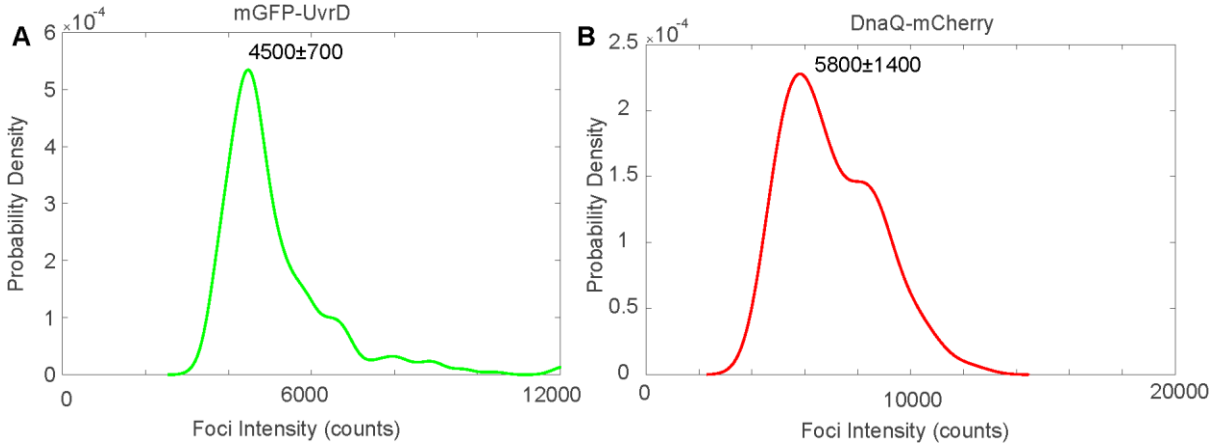

1065

1066 **Supplementary Figure S6: Brightness of single mGFP and mCherry molecules** A. and
1067 B. Characteristic intensity distributions rendered as kernel density estimates of single mGFP-
1068 UvrD and DnaQ-mCherry. Peak±full width at half maximum indicated. Distributions calculated
1069 from the tracked foci intensity distributions from the end of the photobleach process such that
1070 only single fluorophore molecules are detected. Number of molecules per foci before
1071 bleaching is determined by dividing the initial foci intensity by these values for the equivalent
1072 fluorophore.

1073

1074

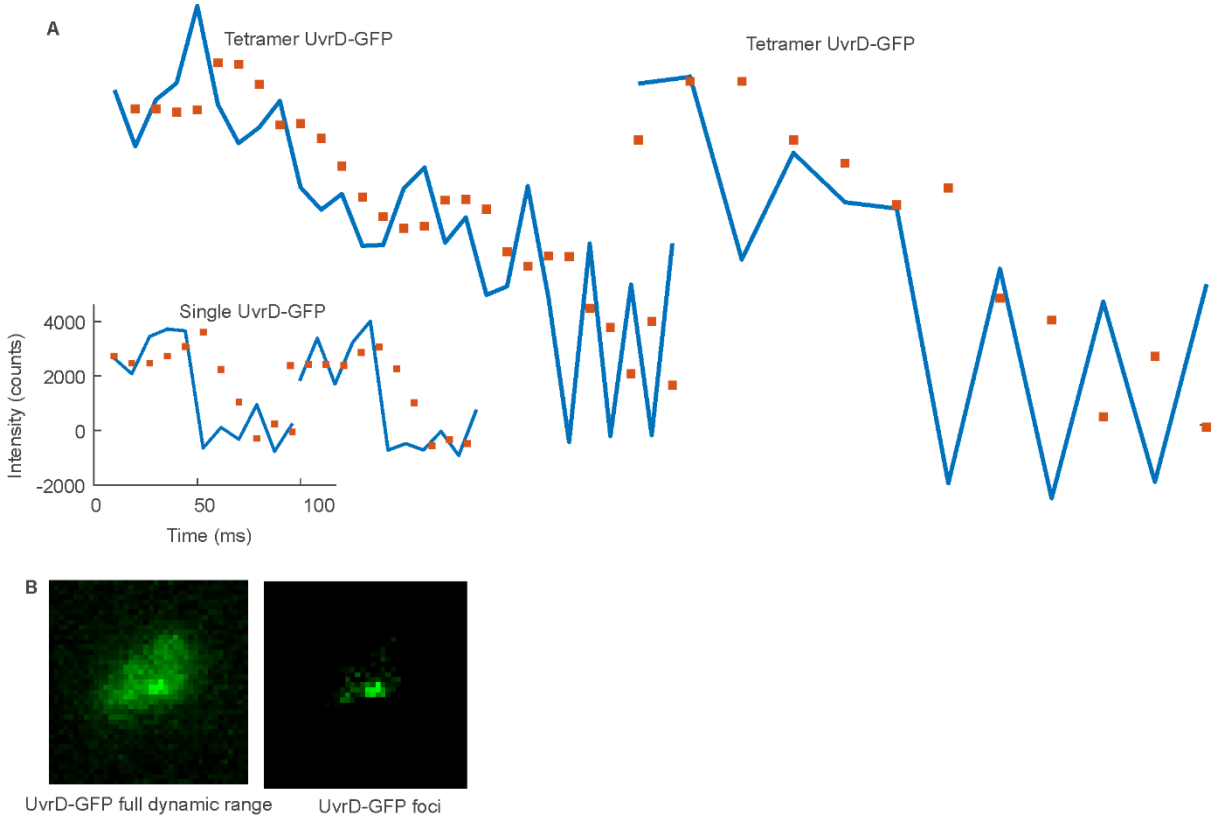

1075
1076
1077 **Supplementary Figure S7: Single-molecule image analysis. A.** Chung-Kennedy filtered
1078 (squares) intensity traces for single UvrD tracks showing tetramers exhibiting multiple
1079 photobleach steps and monomers detected towards the end of photobleaching. Foci were
1080 'overtracked' beyond the last detected bright frame to illustrate steps. **B**. UvrD-GFP
1081 micrograph showing the full dynamic range (left) and adjusted to illustrate a foci (right)
1082

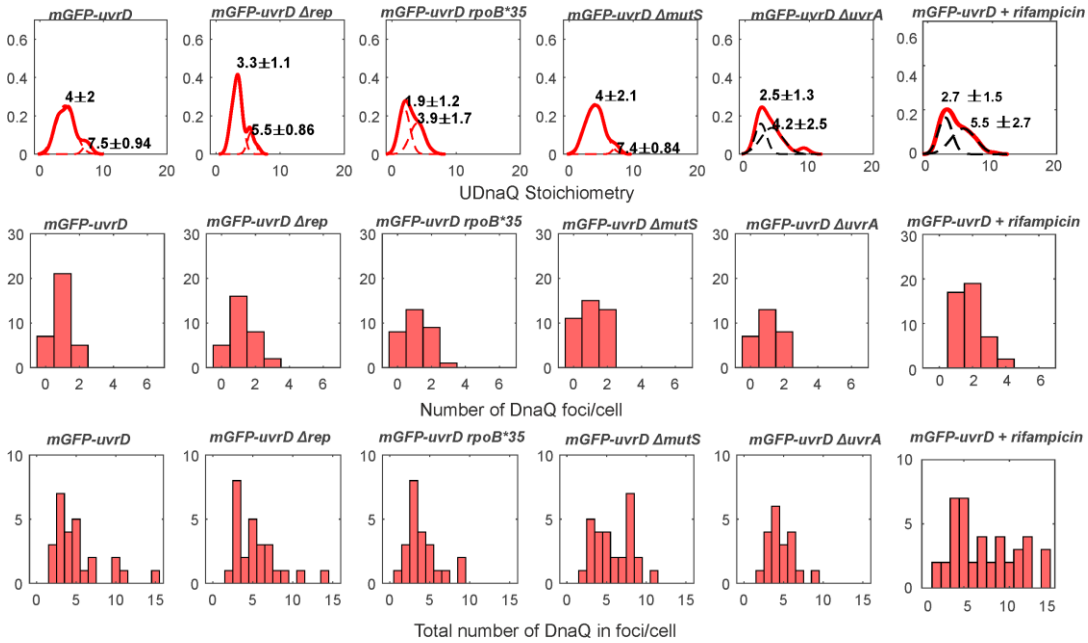

Supplementary Figure S8: DnaQ tracking characterization. Top row: Distribution of DnaQ foci stoichiometry as a kernel density estimate for all strains and conditions (red) with two Gaussian fit overlaid as black dotted lines. Peak ± half width at half maximum shown above. Middle row: Corresponding histogram of number of foci detected per cell. Bottom row: histogram of the total amount of DnaQ in foci per cell. N=30-50 cells per strain or condition.

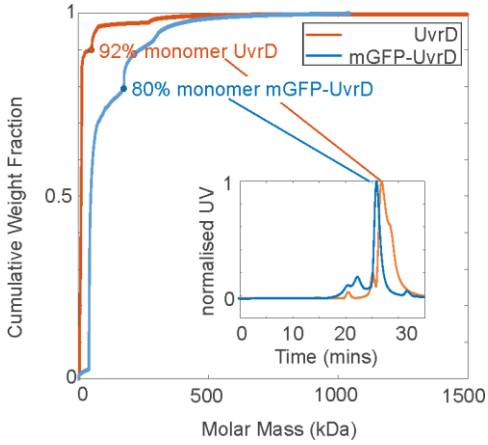

Supplementary Figure S9: SEC-MALLS of UvrD/mGFP UvrD . Size Exclusion Chromatography - Multi-Angle Laser Light Scattering (SEC-MALLS) of 4μM UvrD (red) and mGFP-UvrD (blue) cumulative weight fraction as a function of molar mass. 92% of UvrD and 80% of mGFP-UvrD is consistent with a monomer. Inset shows the normalised UV abosorbance as a function of elution time through the column with the monomer peaks indicated.

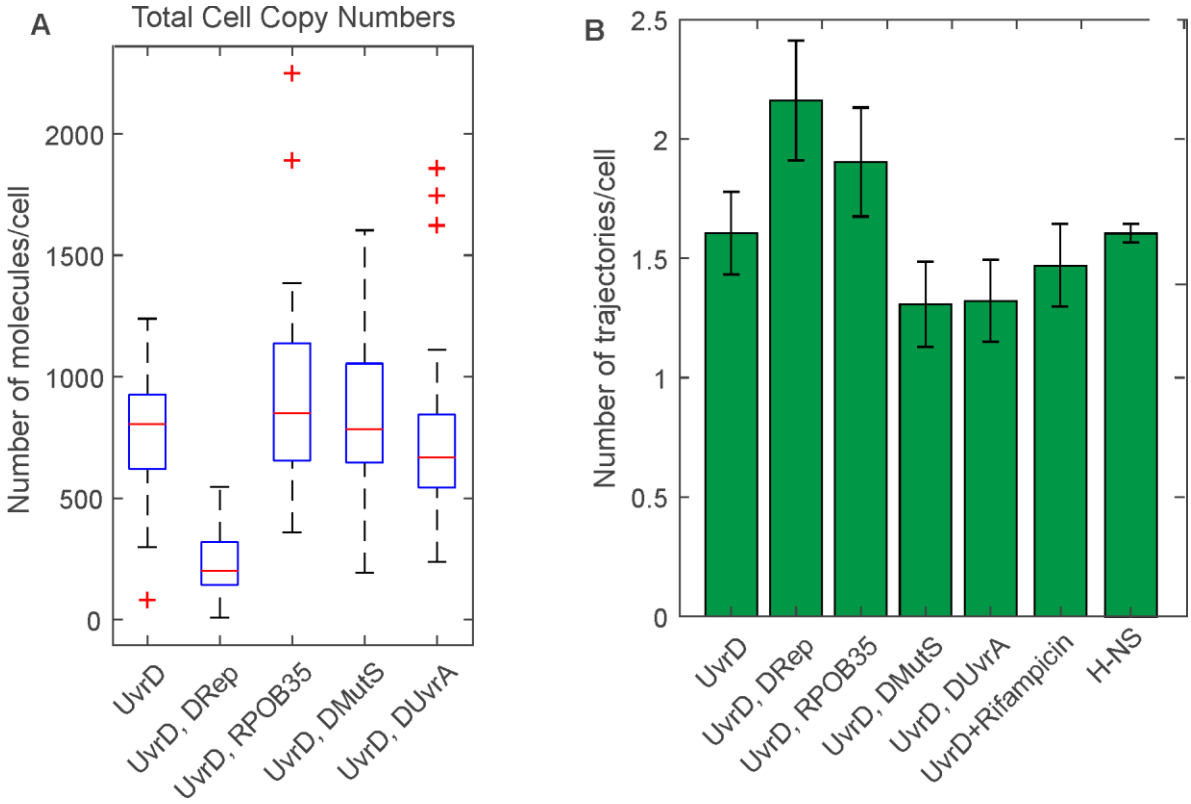

Supplementary Figure S10: A. Boxplot of the total number of mGFP-UvrD molecules per cell, estimated by numerical integration of the whole cell fluorescence. Median is shown as red line, bottom and top of the blue box mark the 25th and 75th percentiles and whiskers extend to the most extreme points not considered outliers (2.7 standard deviations covering 99.3% of normally distributed data) with outliers beyond this shown as red +. N=30 cells per strain. B Number of trajectories per cell used in the stoichiometry determination

1113

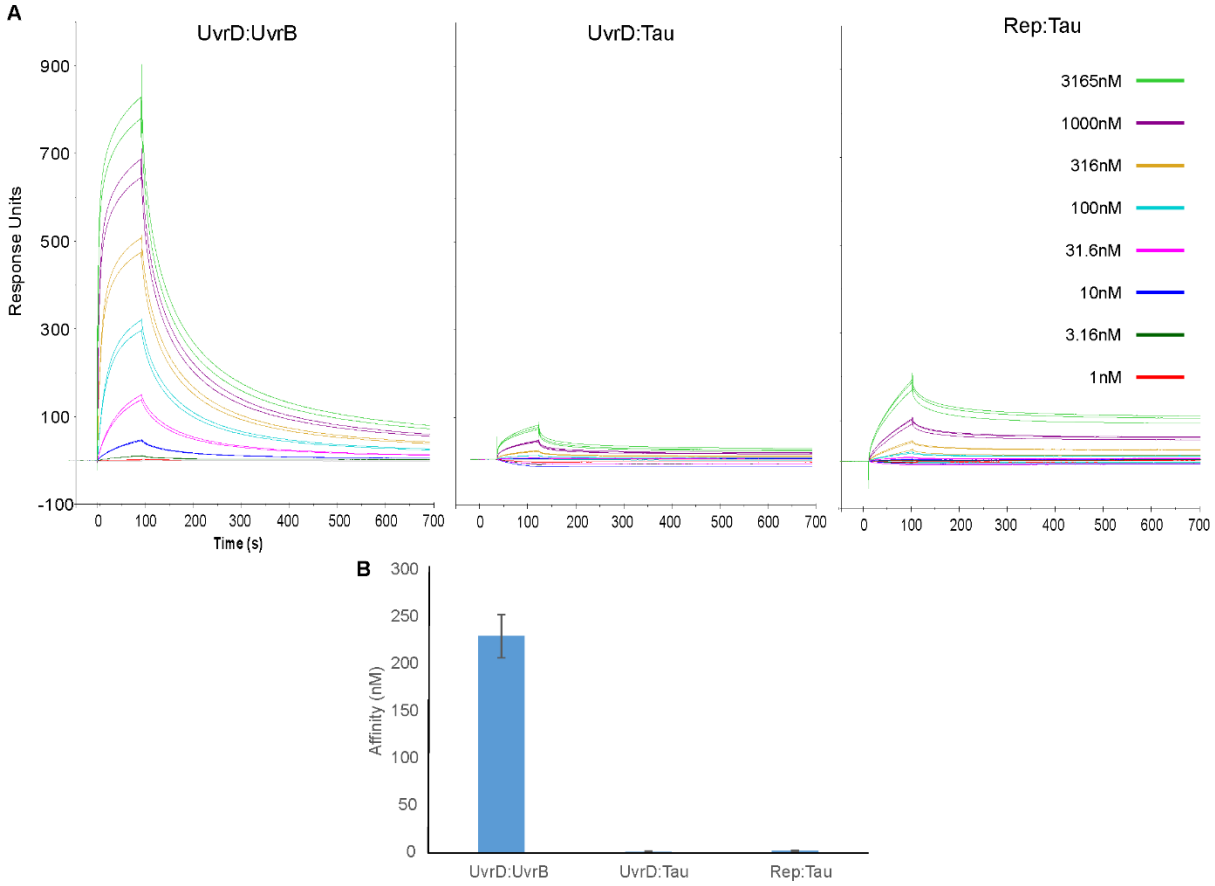

1114

1115 **Supplementary Figure S11: Surface plasmon resonance measurements of helicase**
1116 **interactions with Tau** A. Titration response curves for UvrD:UvrB, UvrD:Tau and Rep:Tau
1117 with their affinities shown in B.

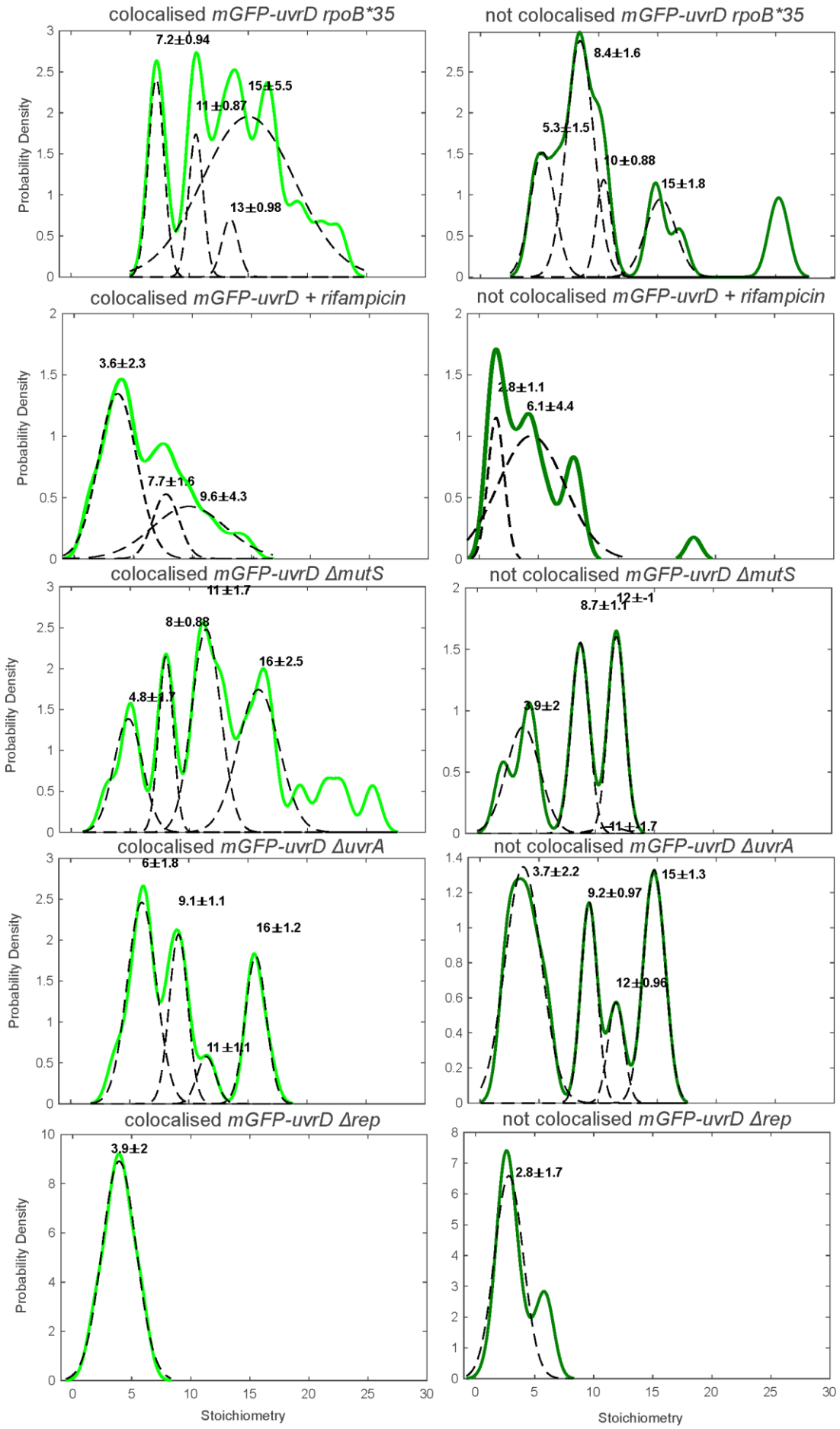
colocalised mGFP-uvrD rpoB*35
7.2±0.94
11±0.87
15±5.5
13±0.98
not colocalised mGFP-uvrD rpoB*35
8.4±1.6
5.3±1.5
10±0.88
15±1.8
colocalised mGFP-uvrD + rifampicin
3.6±2.3
7.7±1.6
9.6±4.3
not colocalised mGFP-uvrD + rifampicin
2.8±1.1
6.1±4.4
colocalised mGFP-uvrD ΔmutS
11±1.7
8±0.88
16±2.5
4.8±1.7
not colocalised mGFP-uvrD ΔmutS
8.7±1.1
12±-1
3.9±2
11±1.7
colocalised mGFP-uvrD ΔuvrA
6±1.8
9.1±1.1
16±1.2
11±1.1
not colocalised mGFP-uvrD ΔuvrA
3.7±2.2
9.2±0.97
15±1.3
12±0.96
colocalised mGFP-uvrD Δrep
3.9±2
not colocalised mGFP-uvrD Δrep
2.8±1.7
Probability Density
Stoichiometry

1118

1119 **Supplementary Figure S12:** Perturbed UvrD stoichiometry. The distribution of UvrD foci
1120 stoichiometry rendered as a kernel density estimate for foci colocalised (Left) and non-
1121 colocalised (Right) with DnaQ foci. Distributions were fitted with multiple Gaussian fits (black
1122 dotted lines) with the peak value ± half width at half maximum indicated above each peak.
1123

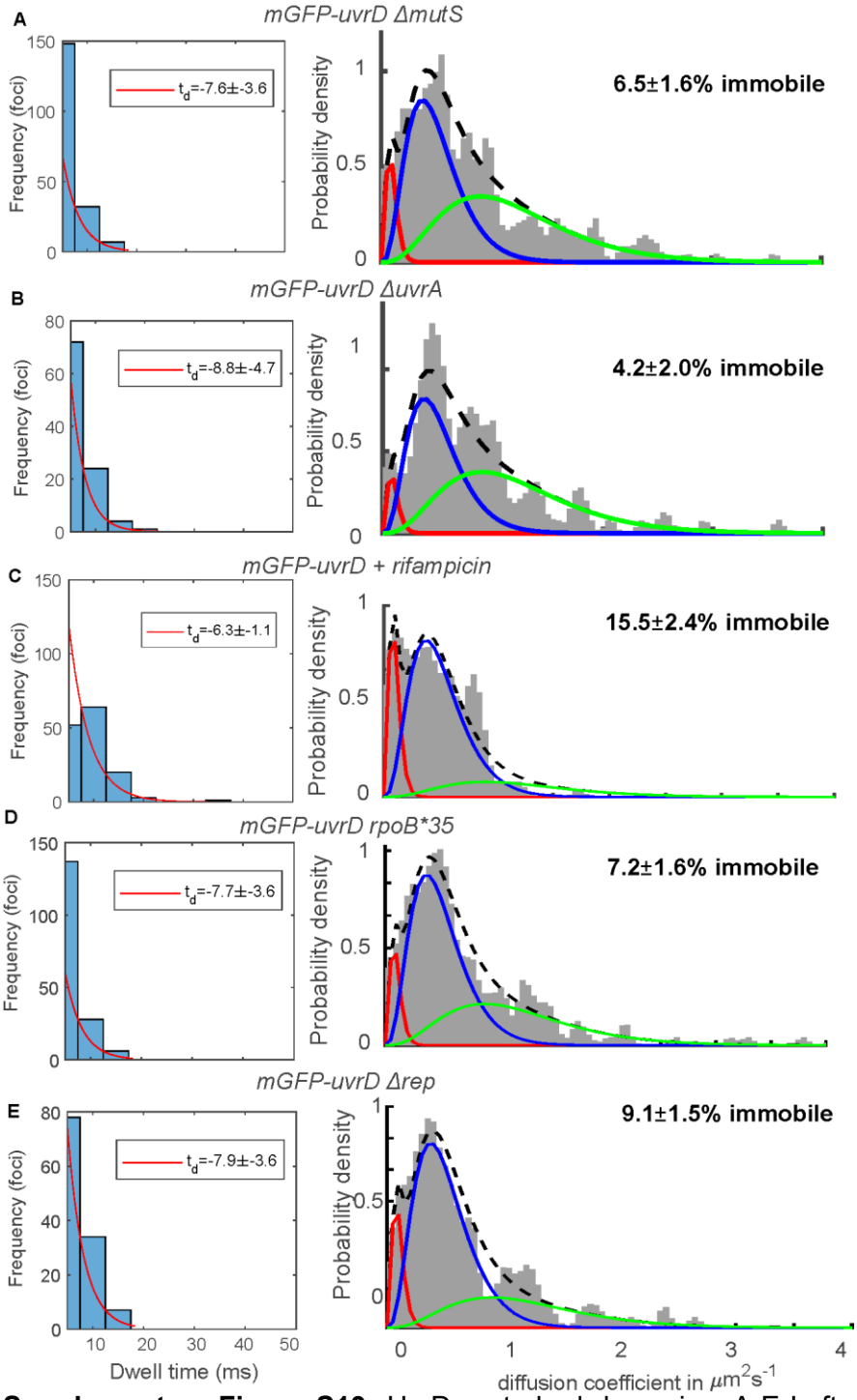

Supplementary Figure S13: UvrD perturbed dynamics. A-E Left, distribution of time UvrD and DnaQ foci were colocalised (blue) fit with an exponential (red) to yield a characteristic dwell time. Right, distribution of microscopic diffusion coefficients of UvrD foci (grey) fitted with a three state gamma distribution model containing a relatively immobile population with D = 0.1 μm^2/s (red), a transiently immobile population, D = 0.5 μm^2/s (blue) and a mobile population, D=1.2 μm^2/s (green). Errors represent 95% confidence intervals. N~300 foci/condition.

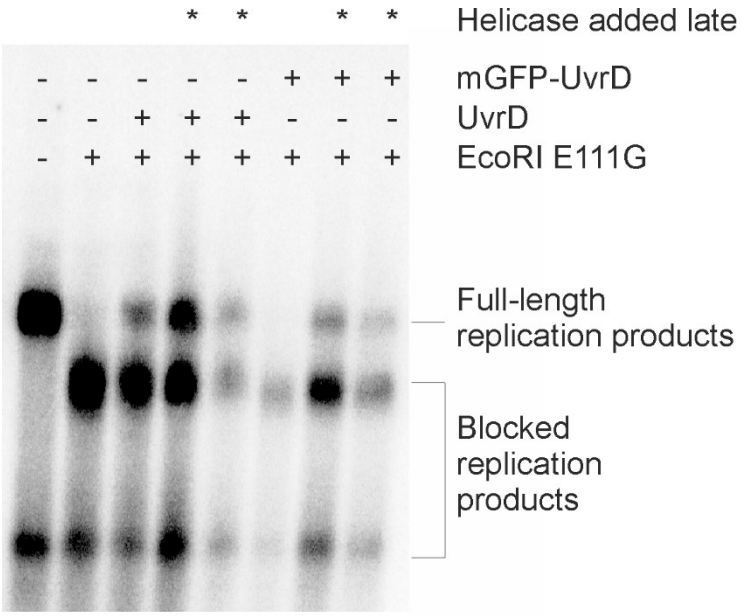

Supplementary Figure S14: In vitro replication assay using mGFP-UvrD. Denaturing agarose gel of replication products formed from pPM872 (1) in the absence and presence of EcoRI E111G block, mGFP-UvrD and UvrD added pre- and post-collision (*) as indicated.

Supplementary references

1. Baba,T., Ara,T., Hasegawa,M., Takai,Y., Okumura,Y., Baba,M., Datsenko,K.A., Tomita,M., Wanner,B.L. and Mori,H. (2006) Construction of Escherichia coli K-12 in-frame, single-gene knockout mutants: the Keio collection. *Mol. Syst. Biol.*, **2**, 2006.0008.
2. Bachmann,B.J. (1996) Derivations and genotypes of some mutant derivatives of Escherichia coli K-12. . In Neidhardt,F.C., Curtiss III,R., Ingraham,J.L., Lin,E.C.C., Low,K.B., Magasanik,B., Reznikoff,W.S., Riley,M., Schaechter,M., Umbarger,H.E. (eds), *Escherichia coli and Salmonella cellular and molecular biology*. ASM Press, Washington, DC, pp. 2460–2488.
3. Bernhardt,T.G. and de Boer,P.A.J. (2004) Screening for synthetic lethal mutants in Escherichia coli and identification of EnvC (YibP) as a periplasmic septal ring factor with murein hydrolase activity. *Mol. Microbiol.*, **52**, 1255–1269.
4. Guy,C.P., Atkinson,J., Gupta,M.K., Mahdi,A.A., Gwynn,E.J., Rudolph,C.J., Moon,P.B., van Knippenberg,I.C., Cadman,C.J., Dillingham,M.S., *et al.* (2009) Rep provides a second motor at the replisome to promote duplication of protein-bound DNA. *Mol. Cell*, **36**, 654–666.
5. Syeda,A.H., Wollman,A.J.M., Hargreaves,A.L., Howard,J.A.L., Brüning,J.-G., McGlynn,P. and Leake,M.C. (2019) Single-molecule live cell imaging of Rep reveals the dynamic interplay between an accessory replicative helicase and the replisome. *Nucleic Acids Res.*, **47**, 6287–6298.
6. Datsenko,K.A. and Wanner,B.L. (2000) One-step inactivation of chromosomal genes in *Escherichia coli* K-12 using PCR products. *Proc. Natl. Acad. Sci. USA*, **97**, 6640–6645.
7. Boubakri,H., de Septenville,A.L., Viguera,E. and Michel,B. (2010) The helicases DinG, Rep and UvrD cooperate to promote replication across transcription units in vivo. *EMBO J.*, **29**, 145–157.
8. Brüning,J.-G., Howard,J.A.L. and McGlynn,P. (2016) Use of streptavidin bound to biotinylated DNA structures as model substrates for analysis of nucleoprotein complex disruption by helicases. *Methods*, **108**, 48–55.
9. Brüning,J.-G., Howard,J.A.L., Myka,K.K., Dillingham,M.S. and McGlynn,P. (2018) The 2B subdomain of Rep helicase links translocation along DNA with protein displacement. *Nucleic Acids Res.*, **46**, 8917–8925.